

# RNAi Suppression of *Arogenate Dehydratase1* Reveals That Phenylalanine Is Synthesized Predominantly via the Arogenate Pathway in Petunia Petals

Hiroshi Maeda,<sup>a</sup> Ajit K Shasany,<sup>a,b</sup> Jennifer Schnepf,<sup>a</sup> Irina Orlova,<sup>a</sup> Goro Taguchi,<sup>c,1</sup> Bruce R. Cooper,<sup>d</sup> David Rhodes,<sup>a</sup> Eran Pichersky,<sup>c</sup> and Natalia Dudareva<sup>a,2</sup>

<sup>a</sup>Department of Horticulture and Landscape Architecture, Purdue University, West Lafayette, Indiana 47907

<sup>b</sup>Central Institute of Medicinal and Aromatic Plants, Lucknow-226015, India

<sup>c</sup>Department of Molecular, Cellular, and Developmental Biology, University of Michigan, Ann Arbor, Michigan 48109

<sup>d</sup>Bindley Bioscience Center, Metabolite Profiling Facility, Purdue University, West Lafayette, Indiana 47907

L-Phe, a protein building block and precursor of numerous phenolic compounds, is synthesized from prephenate via an arogenate and/or phenylpyruvate route in which arogenate dehydratase (ADT) or prephenate dehydratase, respectively, plays a key role. Here, we used *Petunia hybrida* flowers, which are rich in Phe-derived volatiles, to determine the biosynthetic routes involved in Phe formation in planta. Of the three identified petunia ADTs, expression of *ADT1* was the highest in petunia petals and positively correlated with endogenous Phe levels throughout flower development. *ADT1* showed strict substrate specificity toward arogenate, although with the lowest catalytic efficiency among the three ADTs. *ADT1* suppression via RNA interference in petunia petals significantly reduced ADT activity, levels of Phe, and downstream phenylpropanoid/benzenoid volatiles. Unexpectedly, arogenate levels were unaltered, while shikimate and Trp levels were decreased in transgenic petals. Stable isotope labeling experiments showed that *ADT1* suppression led to downregulation of carbon flux toward shikimic acid. However, an exogenous supply of shikimate bypassed this negative regulation and resulted in elevated arogenate accumulation. Feeding with shikimate also led to prephenate and phenylpyruvate accumulation and a partial recovery of the reduced Phe level in transgenic petals, suggesting that the phenylpyruvate route can also operate in planta. These results provide genetic evidence that Phe is synthesized predominantly via arogenate in petunia petals and uncover a novel posttranscriptional regulation of the shikimate pathway.

## INTRODUCTION

In plants, L-Phe is not only a building block for protein synthesis but also a precursor of >8000 phenolic compounds that constitute up to 30 to 45% of plant organic matter (Razal et al., 1996) and have profound impacts on plant growth, development, reproduction, and defense (Croteau et al., 2000). These compounds are widely spread across the plant kingdom and include structural components (e.g., lignin, suberin, and other cell wall-associated phenolics) that provide plants with mechanical support and physical barriers against herbivory and microbial invasion; flavonoid and anthocyanin pigments and phenylpropanoid/benzenoid volatiles that contribute to flower and fruit color and aroma to ensure pollination and seed dispersal;

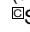
defense molecules (lignans, flavonoids, isoflavonoids, condensed tannins, and some simple phenolic compounds) with antimicrobial and antifeedant properties; UV protectants (flavonoids and other phenolics) for absorbing DNA-damaging UV lights; and signal molecules, such as isoflavonoids and the ubiquitous plant hormone salicylic acid (Ogawa et al., 2005, 2006; Pan et al., 2006; Sawada et al., 2006), although the latter can also be synthesized from isochorismate by a Phe-independent pathway under pathogen attacks (Wildermuth et al., 2001; Catinot et al., 2008).

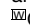
Despite the major roles of Phe in plant physiology and metabolism, our knowledge of its biosynthesis and regulation in plants remains fragmented. Phe is derived from chorismate, the final product of the shikimate pathway (Schmid and Amrhein, 1995; Herrmann and Weaver, 1999). Chorismate is converted by chorismate mutase (CM) to prephenate, which can be subsequently converted to Phe via two alternative pathways (Siehl, 1999; Figure 1). In one pathway, prephenate undergoes transamination to arogenate, which is then dehydrated/decarboxylated to Phe by arogenate dehydratase (ADT; EC 4.2.1.91). In the other route, prephenate is first subjected to dehydration/decarboxylation catalyzed by prephenate dehydratase (PDT; EC 4.2.1.51) to form phenylpyruvate, which is then transaminated to Phe (Siehl, 1999). Most microorganisms studied to date synthesize Phe via phenylpyruvate and contain PDTs (Davidson et al., 1972; Bentley, 1990; Kleeb et al., 2006), with a few exceptions (e.g., *Euglena gracilis* and

<sup>1</sup> Current address: Division of Applied Biology, Faculty of Textile Science and Technology, Shinshu University, 3-15-1 Tokida, Ueda 386-8567, Japan.

<sup>2</sup> Address correspondence to dudareva@purdue.edu.

The author responsible for distribution of materials integral to the findings presented in this article in accordance with the policy described in the Instructions for Authors (www.plantcell.org) is: Natalia Dudareva (dudareva@purdue.edu).

 Some figures in this article are displayed in color online but in black and white in the print edition.

 Online version contains Web-only data.

www.plantcell.org/cgi/doi/10.1105/tpc.109.073247

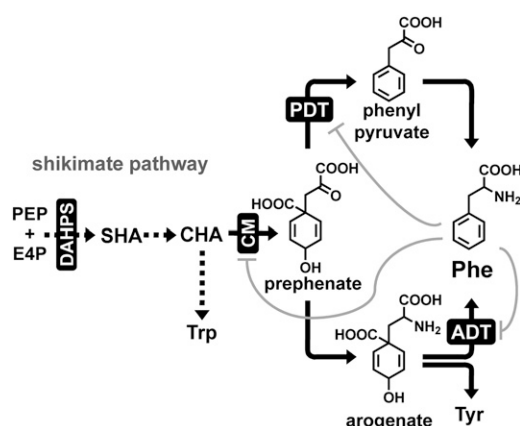


**Figure 1.** Proposed Biosynthetic Pathways Leading to Phe in Plants.

Dotted arrows indicate involvement of multiple enzymatic steps. Gray lines denote feedback inhibition. CHA, chorismate; DAHPS, 3-deoxy-D-arabino-heptulosonate 7-phosphate synthase; E4P, erythrose 4-phosphate; PEP, phosphoenolpyruvate; SHA, shikimate.

*Pseudomonas diminuta*), which possess ADTs (Byng et al., 1981; Zamir et al., 1985). In *Escherichia coli*, the *PheA* gene encodes a bifunctional enzyme carrying both PDT and CM activities (with a CM domain fused to the N-terminal end of the PDT domain; Davidson et al., 1972; Zhang et al., 1998), and the null mutations in the PDT domain result in a Phe auxotrophic mutant (Simmonds, 1950; Davis, 1953; Katagiri and Sato, 1953), suggesting that Phe biosynthesis in *E. coli* occurs exclusively via phenylpyruvate (Bentley, 1990).

In plants, PDT activity has been detected only in etiolated *Arabidopsis thaliana* seedlings (Warpeha et al., 2006), while ADT activities have been reported in a broad variety of plants (Jung et al., 1986; Siehl and Conn, 1988). In addition, recent biochemical characterization of six ADT genes from *Arabidopsis* and one (out of four) from rice (*Oryza sativa*) revealed that three *Arabidopsis* dehydratases have strict substrate specificity toward aroenate, while the remaining three, as well as the rice enzyme, can also accept prephenate, albeit with 10- to 100-fold lower catalytic efficiencies (Cho et al., 2007; Yamada et al., 2008). The genetic redundancy of *Arabidopsis* and rice ADTs, the lack of their absolute substrate specificity (Cho et al., 2007; Yamada et al., 2008), the inability to detect unstable pathway intermediates (e.g., aroenate and prephenate) from plant tissues (Razal et al., 1994), and the indispensable nature of Phe make it difficult to determine the physiological roles of ADT/PDTs in planta. As a result, there is no genetic evidence indicating which of the two proposed biosynthetic pathways (or both) is involved in Phe biosynthesis in plants.

To address this question, we took advantage of the fact that *Petunia hybrida* petals produce a large quantity of Phe-derived volatiles (Verdonk et al., 2003; Boatright et al., 2004). Genetic perturbations of Phe levels in this particular organ using a tissue-specific promoter allow us to investigate Phe biosynthetic pathways without affecting plant growth and development. Using an RNA interference (RNAi) approach to suppress ADT with strict substrate specificity toward aroenate, we provide in planta

evidence that Phe is predominantly produced via aroenate in petunia petals. Analysis of key pathway intermediates in transgenic and control petals further revealed unexpected posttranscriptional feedback regulation of the shikimate pathway leading to Phe biosynthesis.

## RESULTS

### Identification of Petunia Genes Encoding ADT/PDT

To identify the gene(s) encoding ADT/PDT expressed in petunia petals, we searched our previously generated petunia petal-specific EST database (Boatright et al., 2004), as well as those available at the Sol genomics network (<http://www.sgn.cornell.edu>), for sequences with homology to *E. coli* CM/PDT (Hudson and Davidson, 1984) or *Arabidopsis* ADTs (Cho et al., 2007). A total of 41 ESTs were identified and assembled into two contigs and one singlet each represented by 36, 1, and 4 ESTs and designated as *P. hybrida* ADT1, ADT2, and ADT3 (see below), respectively. The contigs for petunia ADT1 and ADT3 contain full-length open reading frames, whereas the ADT2 singlet was truncated at its 5' end and the corresponding full-length sequence was recovered by 5' rapid amplification of cDNA ends. The resulting cDNAs encode proteins of 424, 394, and 434 amino acids with predicted molecular masses of 45.9, 43.4, and 47.3 kD, respectively. The ADT1 and ADT3 proteins were highly similar to each other (84% amino acid identity), while ADT2 exhibited only 68 to 69% amino acid identity to ADT1 and ADT3 (see Supplemental Figure 1 online). Petunia ADT1, ADT2, and ADT3 showed 78, 77, and 80% amino acid identity to their closest *Arabidopsis* homologs, At ADT3, At ADT2, and At ADT6, respectively (Figure 2; see Supplemental Data Set 1 online). Amino acid sequence alignments of newly identified petunia ADTs with *E. coli* CM/PDT, as well as with known and putative

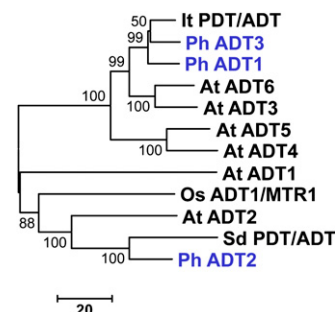


**Figure 2.** Phylogenetic Tree of Plant ADTs and PDTs.

Phylogenetic tree illustrating relatedness of petunia ADTs (Ph ADTs) to other plant ADTs/PDTs. The distance bar representing percentage of sequence differences is shown under the tree. The bootstrap values calculated from 1000 replicates are given for the nodes. Only a subset of PDTs/ADTs with high amino acid homology to petunia ADTs is shown. At ADT1 to At ADT6, *Arabidopsis thaliana* ADT1 to ADT6; Os ADT/MTR1, *Oryza sativa* ADT/MTR1; It PDT/ADT, *Ipomoea trifida* putative PDT/ADT; Sd PDT/ADT, *Solanum demissum* putative PDT/ADT.

[See online article for color version of this figure.]

plant PDT/ADTs, revealed the presence of two highly conserved regions corresponding to the ADT/PDT catalytic and Phe binding regulatory ACT (named after the regulatory domains of Asp kinase, CM, and prephenate dehydrogenase TyrA) domains (see Supplemental Figure 1 online; Grant, 2006). Comparison with putative ADT/PDT sequences of cyanobacteria revealed that the petunia ADT proteins, as well as other plant ADT/PDTs, contain an additional 100 to 140 amino acids in their N terminus, a part of which was predicted to be a putative plastid transit peptide by both ChloroP 1.1 (cbs.dtu.dk/services/ChloroP) and WoLF PSORT (wolfsort.seq.cbrc.jp).

### Biochemical Characterization of Petunia ADTs

The coding regions corresponding to mature ADT proteins (lacking the N-terminal plastid transit peptides) were subcloned into the expression vector pET-28a, which contains an N-terminal hexahistidine (6xHis) tag. Recombinant proteins were expressed in *E. coli*, purified, and analyzed for dehydratase activities with aroenate and prephenate as substrates. Since *E. coli* crude extract contains endogenous PDT activity (see Supplemental Figure 2 online) derived from a bifunctional CM/PDT enzyme (Davidson et al., 1972; Zhang et al., 1998), CM activity was carefully monitored to ensure the absence of *E. coli* CM/PDT contamination in purified fractions (see Supplemental Figure 2 online). All three petunia recombinant proteins were able to convert aroenate to Phe with apparent  $K_m$  values of 179, 66.7, and 48.8  $\mu\text{M}$  for ADT1, ADT2, and ADT3, respectively (Table 1). ADT2 exhibited the highest catalytic efficiency ( $k_{\text{cat}}/K_m$  ratio) with this substrate ( $18.5 \text{ mM}^{-1} \text{ s}^{-1}$ ), which was 12- and almost 5-fold higher than that of ADT1 ( $1.5 \text{ mM}^{-1} \text{ s}^{-1}$ ) and ADT3 ( $4.0 \text{ mM}^{-1} \text{ s}^{-1}$ ), respectively (Table 1). Petunia ADT2 and ADT3 could also use prephenate as substrate with apparent  $K_m$  values of 752 and 465  $\mu\text{M}$ . Their catalytic efficiencies of 0.08 and 0.03  $\text{mM}^{-1} \text{ s}^{-1}$ , respectively, were 10- to 200-fold lower than the corresponding values with aroenate (Table 1). Based on the exclusive substrate specificity of ADT1 and preferred substrate specificity of ADT2 and ADT3 for aroenate, these petunia enzymes were designated as ADTs.

**Table 1.** Kinetic Parameters of Petunia ADTs

	ADT1	ADT2	ADT3
<b>Aroenate<sup>a</sup></b>			
$K_m$ ( $\mu\text{M}$ )	$179.0 \pm 15.5$	$66.7 \pm 10.2$	$48.8 \pm 7.2$
$V_{\text{max}}$ (pkat/mg)	$6,234 \pm 912$	$30,277 \pm 5,855$	$4,464 \pm 616$
$k_{\text{cat}}$ ( $\text{s}^{-1}$ )	$0.267 \pm 0.039$	$1.231 \pm 0.238$	$0.194 \pm 0.027$
$k_{\text{cat}}/K_m$ ( $\text{mM}^{-1} \text{ s}^{-1}$ )	$1.48 \pm 0.12$	$18.51 \pm 2.23$	$4.00 \pm 0.31$
<b>Prephenate<sup>a</sup></b>			
$K_m$ ( $\mu\text{M}$ )	n.d. <sup>b</sup>	$752.0 \pm 70.3$	$465.8 \pm 18.8$
$V_{\text{max}}$ (pkat/mg)	n.d.	$1,473 \pm 197$	$280 \pm 10$
$k_{\text{cat}}$ ( $\text{s}^{-1}$ )	n.d.	$0.060 \pm 0.008$	$0.012 \pm 0.000$
$k_{\text{cat}}/K_m$ ( $\text{mM}^{-1} \text{ s}^{-1}$ )	n.d.	$0.08 \pm 0.01$	$0.03 \pm 0.00$

Data are means  $\pm$  SE ( $n = 3$  independent experiments).

<sup>a</sup>Substrates used.

<sup>b</sup>Not detectable.

### Endogenous Phe and ADT Transcript Levels in Petunia Flowers

Emission of Phe-derived phenylpropanoid/benzenoid volatiles from petunia flowers begins after anthesis and changes rhythmically during a daily light/dark cycle (Kolosova et al., 2001; Verdonk et al., 2003). To examine whether these changes in the volatile profile correlate with Phe levels, endogenous Phe pools were analyzed during the day (11 AM) and night (8 PM) in petals harvested from 1 d before to 6 d after anthesis. While daytime Phe levels increased only slightly during flower development, nighttime levels increased drastically after anthesis, reached the highest level on day 2 after anthesis, and gradually declined thereafter to 56% of the maximum level at the end of the life span of the flower (Figure 3A). A detailed analysis of the Phe levels over two daily light/dark cycles revealed oscillations with a maximum at night, between 11 PM and 3 AM, followed by a decrease to basal level by 7 AM (Figure 3B), positively correlating with volatile emission (Kolosova et al., 2001; Verdonk et al., 2003).

To assess the involvement of ADT1, ADT2, and ADT3 in the biosynthesis of Phe required for phenylpropanoid/benzenoid formation in petunia flowers, their tissue- and organ-specific expression was examined using quantitative RT-PCR (qRT-PCR) with gene-specific primers. Out of three ADTs, ADT1 exhibited the highest level of expression in corolla and tube, the scent-producing parts of petunia flowers. In corolla, the ADT1 transcript levels exceeded those of ADT2 and ADT3 by 88- and 10-fold, respectively (Figure 3E). Low levels of expression were found for all three ADTs in other flower organs and leaves. In stem tissue, a site of active lignin biosynthesis, only ADT1 and ADT3 were expressed, but their levels were 41- and 56-fold lower, respectively, than the ADT1 level in corolla (Figure 3E). The mRNA levels of ADT1 and to a lesser extent of ADT3 were developmentally regulated in flower corolla, peaking at 3 d after anthesis (Figure 3C). Moreover, their expression levels changed rhythmically during a daily light/dark cycle, peaking at 7 PM (Figure 3D) and preceding the peaks of Phe levels (Figure 3B) and phenylpropanoid/benzenoid emission (Kolosova et al., 2001; Verdonk et al., 2003; Boatright et al., 2004). High ADT1 transcript levels in corolla and tubes imply that ADT1 plays a major role in Phe biosynthesis in petunia petals.

### Subcellular Localization of Petunia ADTs

Analysis of the ADT1, ADT2, and ADT3 protein sequences predicted the presence of N-terminal plastid transit peptides of 52, 47, and 43 amino acids, respectively (ChloroP; see Supplemental Figure 1 online). To experimentally determine the subcellular localization of the petunia ADT proteins, the complete coding regions of each gene, as well as the individual N-terminal transit peptides, were fused to a green fluorescent protein (GFP) reporter gene, and the resulting constructs were transferred to *Arabidopsis* protoplasts where the corresponding transient GFP expression was analyzed by confocal scanning microscopy (Figure 4). GFP fluorescence exhibited punctate and discrete patterns associated with the chloroplasts when full-length proteins were fused to GFP (Figures 4A, 4C, and 4E). However, when the first 80, 75 and 79 amino acids of ADT1, ADT2, and ADT3,

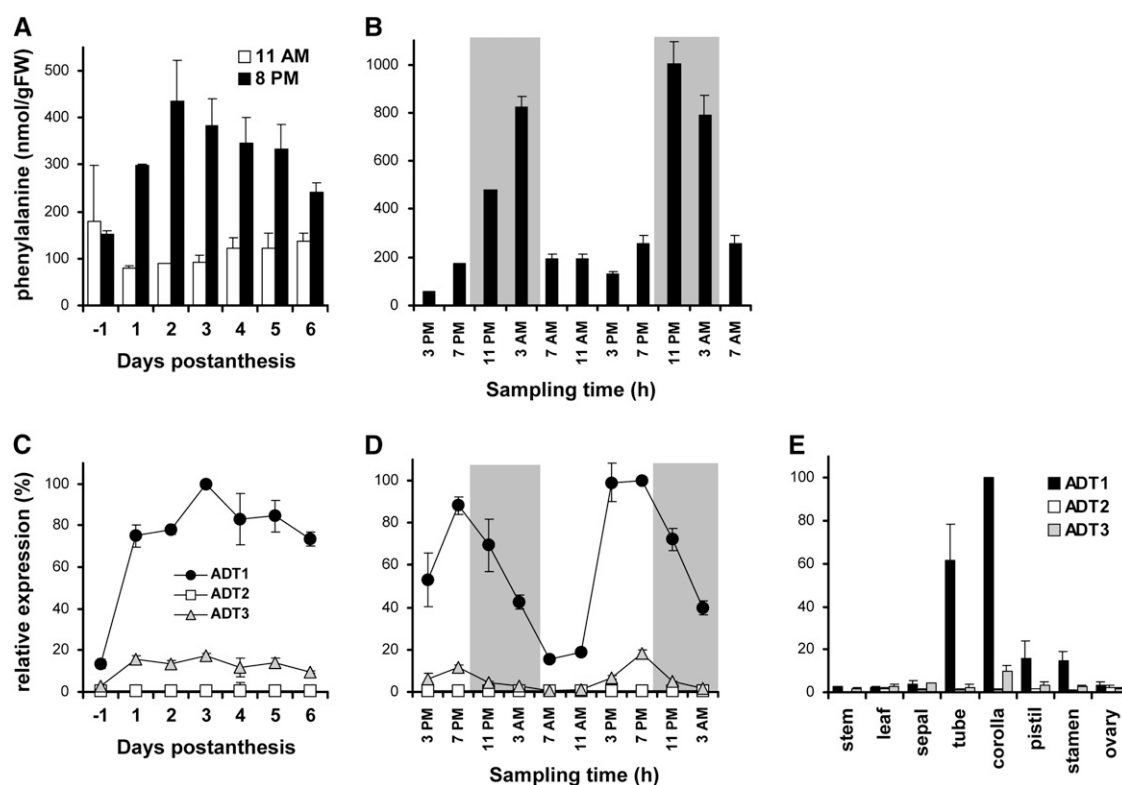


**Figure 3.** Endogenous Phe Levels and Expression Profiles of *ADT* Genes in Petunia.

**(A)** Endogenous Phe pools in petunia corolla at different stages of flower development starting from 1 d before opening (flower buds) to day 6 postanthesis. At each developmental stage, tissue was collected at 11 AM (open bars) and 8 PM (solid bars). Data are means  $\pm$  SE ( $n = 3$  biological replicates with the exception of the 11 AM time point on day 2, which was obtained from a single experiment).

**(B)** Endogenous Phe pools in the corolla of flowers 1 to 3 d postanthesis during a normal light/dark cycle. The corresponding dark periods (9 PM to 6 AM) are shown with gray backgrounds. Data are means  $\pm$  SE ( $n = 3$  or 4 biological replicates with the exception of the first four time points, which were obtained from two experiments).

**(C)** Transcript levels of *ADT1*, *ADT2*, and *ADT3* were determined by qRT-PCR in corolla harvested at different stages of flower development from mature buds to day 6 postanthesis. Data are presented as relative to the 3-d *ADT1* level. Data are means  $\pm$  SE ( $n = 3$  biological replicates).

**(D)** Changes in individual *ADT* transcripts in the corolla of flowers 1 to 3 d postanthesis during a normal light/dark cycle. The dark cycles (9 PM to 6 AM) are shown with gray backgrounds. Data are presented as relative to *ADT1* level at 7 PM on day 2 postanthesis. Data are means  $\pm$  SE ( $n = 3$  biological replicates).

**(E)** Tissue-specific expression of individual *ADTs* shown relative to corolla *ADT1* levels. Data are means  $\pm$  SE ( $n = 3$  biological replicates).

respectively, were fused to GFP, the GFP fluorescence was localized evenly throughout the plastids (Figures 4B, 4D, and 4F), which was similar to that of GFP fused to the transit peptide of ribulose-1,5-bis-phosphate carboxylase/oxygenase (Rubisco) small subunit, which localized in the stroma (Figure 4G), and clearly distinct from the GFP control, which localized in the cytosol (Figure 4H). These results indicate that, similar to the six *Arabidopsis* ADT proteins (Rippert et al., 2009), all petunia ADTs are localized in plastids where Phe biosynthesis takes place (Jung et al., 1986; Siehl et al., 1986).

### RNAi Suppression of *ADT1* in Petunia Petals

To investigate the *in vivo* function of *ADT1* in petunia flowers, its mRNA levels were reduced in petals via an RNAi approach. The RNAi construct was generated using a 444-bp fragment within

the 5' end of the *ADT1* coding region and expressed under the control of the predominantly petal-specific *LIS* (linalool synthase) promoter from *Clarkia breweri* (Cseke et al., 1998). Twenty-nine independent transformants were generated with varying degrees of *ADT1* mRNA suppression relative to untransformed control flower petals (Figure 5A). Four analyzed *ADT1*-RNAi lines (B, C, I, and J) with reduced *ADT1* expression exhibited a reduction in total volatile emission by 25 to 70% relative to the control (Figures 5B and 5C). Two independent lines with the greatest reduction in *ADT1* gene expression (lines B and C) were selected for further metabolic analysis of emitted floral volatiles as well as internal pools of intermediates and end products. The analyses were conducted using petunia petals harvested at 8 PM from flowers 2 d after anthesis (hereafter referred to as 2-d-old petals). The *ADT1*-RNAi construct specifically decreased *ADT1* expression but not *ADT2* and *ADT3* (Figure 6A) and did not alter overall

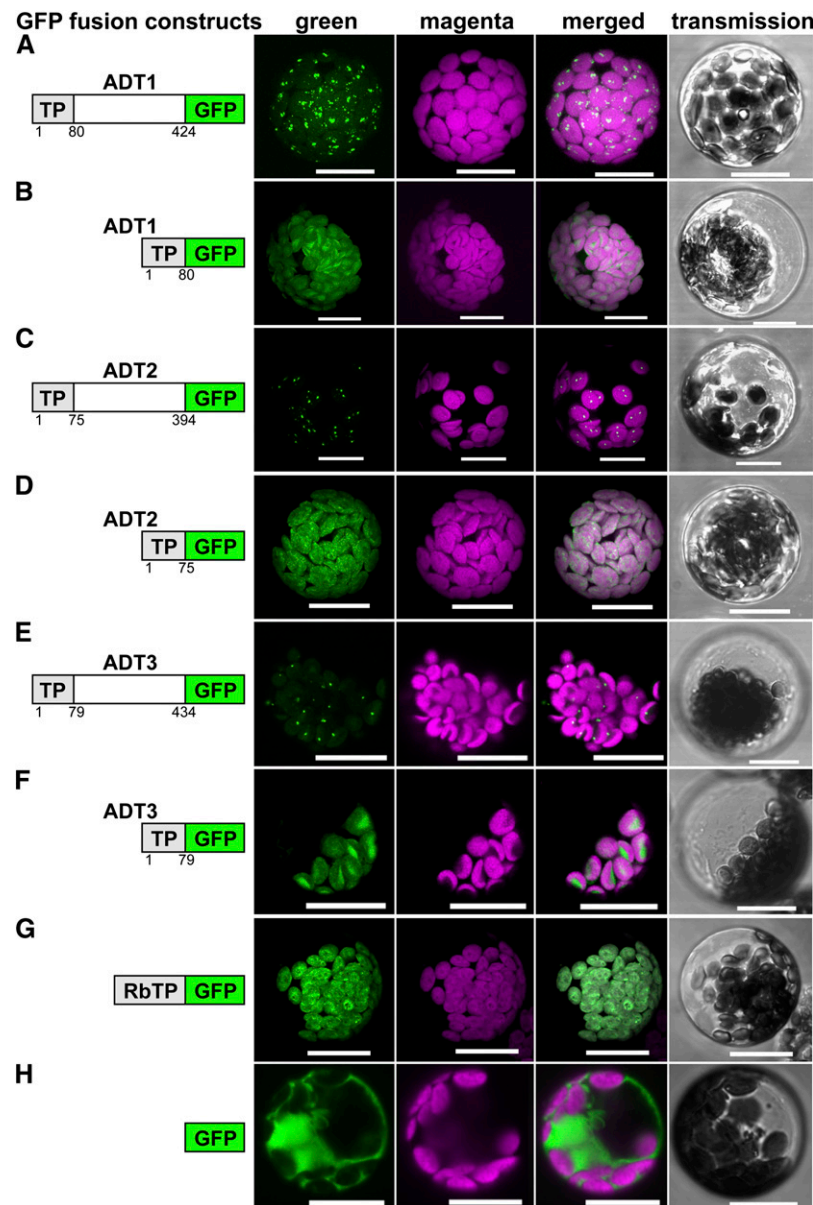


**Figure 4.** Subcellular Localization of Petunia ADT Proteins.

Schematic diagrams of GFP fusion constructs for ADT1 ([A] and [B]), ADT2 ([C] and [D]), and ADT3 ([E] and [F]) are shown on the far left and corresponding transient expression in *Arabidopsis* protoplasts detected by confocal laser scanning microscopy is shown on the right. GFP fluorescence and chlorophyll autofluorescence are shown in the green and magenta vertical panels, respectively. The merged and transmission vertical panels show the two combined fluorescence images and light microscopy images of intact protoplasts, respectively. GFP only (H) and RbTP (Rubisco transit peptide)-GFP fusion (G) are used as cytosolic and chloroplast markers, respectively. The numbers below the fusion constructs show amino acid positions. TP, transit peptide. Bars = 50  $\mu$ m.

morphology, fresh weight, and total protein content in transgenic flowers, which were not different from those of control flowers (Figure 6B). Consistent with the reduced ADT1 expression, ADT1-RNAi lines exhibited a significant reduction in ADT activity (by 58 to 61%) in petal protein extracts relative to controls (Figure 6B), while PDT activity was undetectable under the conditions tested. Furthermore, the endogenous Phe levels in the petals of

these ADT1-RNAi lines were reduced by 75 to 82% relative to controls (Figure 7; see Supplemental Table 1 online), indicating that ADT1 is involved in the biosynthesis of Phe in vivo.

To determine the impact of Phe reduction on the production of phenylpropanoid/benzenoid volatiles, their emission was measured during the night from 8 PM to 8 AM using 2-d-old flowers of both lines B and C and compared with untransformed controls.

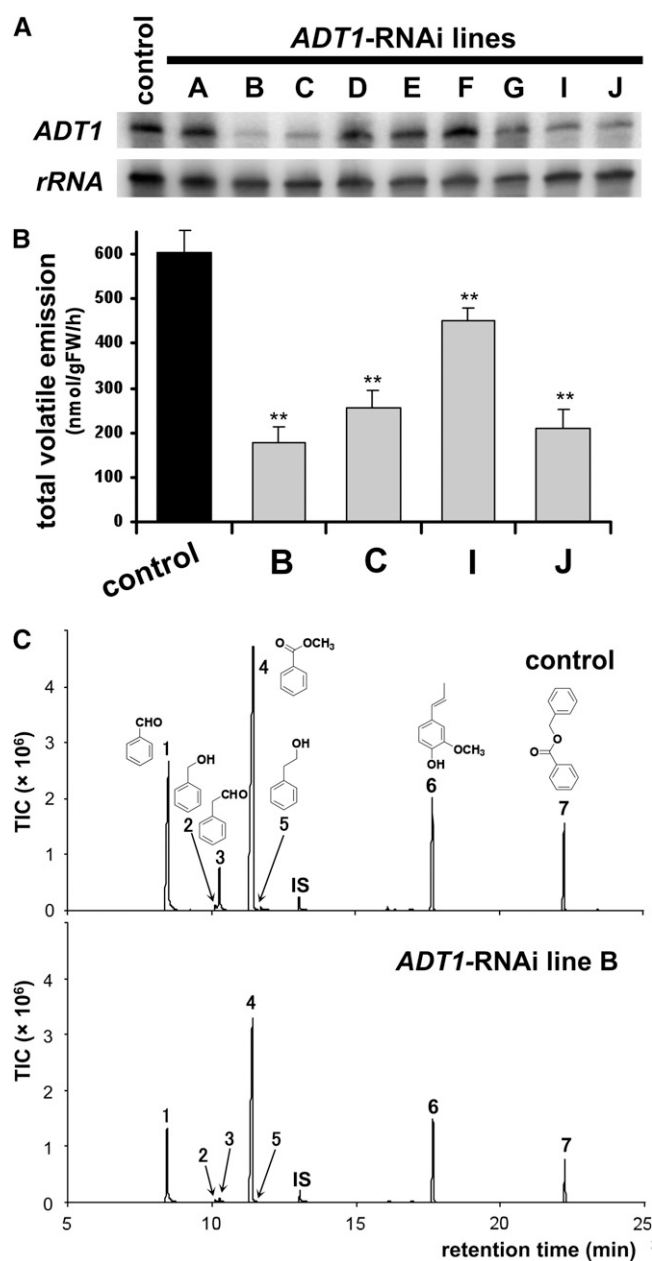


**Figure 5.** Effect of *ADT1* RNAi Suppression on *ADT1* Gene Expression and Volatile Emission from Petunia Flowers.

**(A)** *ADT1* mRNA in the corolla of control and different transgenic *ADT1*-RNAi petunia plants (lines A to J). Total RNA (5 mg per lane) isolated from the corolla limbs of control and independent transgenic flowers (letters on top of the gel) harvested 2 d postanthesis were hybridized with the *ADT1* probe and subsequently rehybridized with an 18S rDNA probe (bottom gel) as a loading control.

**(B)** Total emission of benzenoid and phenylpropanoid compounds from control and transgenic *ADT1*-RNAi petunia flowers harvested 2 d postanthesis. Floral volatiles were collected from 8 PM to 8 AM. The letters represent independent transgenic lines. Data are means  $\pm$  SE ( $n = 6$  to 13). \*\*  $P < 0.01$  by Student's *t* test of transgenics relative to the control.

**(C)** GC-MS chromatograms showing changes in the benzenoid/phenylpropanoid volatile profiles of control (top) and *ADT1*-RNAi line B (bottom)

Emission of all phenylpropanoids/benzenoids was reduced in both lines relative to controls, but the degree of reduction varied among the different compounds (Figure 7; see Supplemental Table 1 online). While phenylacetaldehyde, phenylethanol, benzylacetate, benzaldehyde, and benzylalcohol levels were reduced to 10 to 20% of their levels in control flowers, methylbenzoate, benzylbenzoate, phenylethylbenzoate, and eugenol were only reduced to 30 to 50%. Among all produced volatile compounds, isoeugenol was the least affected by *ADT1* RNAi suppression, and its level in transgenic flowers remained relatively high, 70 to 80% of control flowers (Figure 7; see Supplemental Table 1 online). Consistent with the decrease in emission levels, the endogenous pools of phenylpropanoids/benzenoids in 2-d-old flowers harvested at 8 PM were also reduced, with some compounds decreasing to below the detection limit in line B when compared with controls (e.g., phenylacetaldehyde and phenylethanol; see Supplemental Table 1 online). However, activities of scent-producing enzymes, including phenylacetaldehyde synthase (PAAS; Kaminaga et al., 2006), benzoic acid/salicylic acid carboxyl methyltransferase (BSMT; Negre et al., 2003; Underwood et al., 2005), isoeugenol synthase (IGS; Koeduka et al., 2006), and benzoyl-CoA:benzyl alcohol/phenylethanol benzoyltransferase (BPBT; Boatright et al., 2004), responsible for phenylacetaldehyde, methylbenzoate, isoeugenol, and benzylbenzoate formation, respectively, remained unaltered in transgenic petals (Table 2). Feeding of transgenic RNAi line B flowers with 300  $\mu$ mol exogenous Phe for 4 h (from 8 PM to 12 AM) recovered emission of all volatiles (Figure 8). As a trend, compounds showing a greater reduction in emission under limited Phe conditions in transgenic petals (e.g., benzaldehyde and phenylacetaldehyde; Figure 8; see Supplemental Table 1 online) exhibited greater recovery after exogenous Phe feeding than compounds less affected by *ADT1* mRNA suppression (e.g., methylbenzoate and isoeugenol). These results suggest that limited Phe levels are responsible for the reduced volatile emission in transgenic flowers.

Reduction of Phe levels in *ADT1*-RNAi lines also affected the amount of organic acid intermediates in the phenylpropanoid/benzenoid network. In RNAi line B, the levels of *trans*-cinnamic acid and benzoic acid were reduced by 86 and 77% relative to control, respectively (Figure 7; see Supplemental Table 1 online), while activities of Phe ammonia lyase (PAL) and benzaldehyde dehydrogenase (BALDH; Long et al., 2009), which are responsible for the formation of respective organic acids, remained unchanged in transgenic petals (Table 2). Caffeic and ferulic acid levels were reduced by only 45 and 38%, respectively, consistent with  $\sim$ 30% reduction in the isoeugenol emission relative to controls (Figure 7; see Supplemental Table 1 online). Similar changes were also observed in petals of transgenic line C (Figure 7; see Supplemental Table 1 online). The level of salicylic acid

flowers. Total ion currents (TIC) are shown. Compounds were identified based on their mass spectra and retention time of respective authentic standards: 1, benzaldehyde; 2, benzyl alcohol; 3, phenylacetaldehyde; 4, methylbenzoate; 5, 2-phenylethanol; IS, internal standard (naphthalene); 6, isoeugenol; 7, benzylbenzoate.



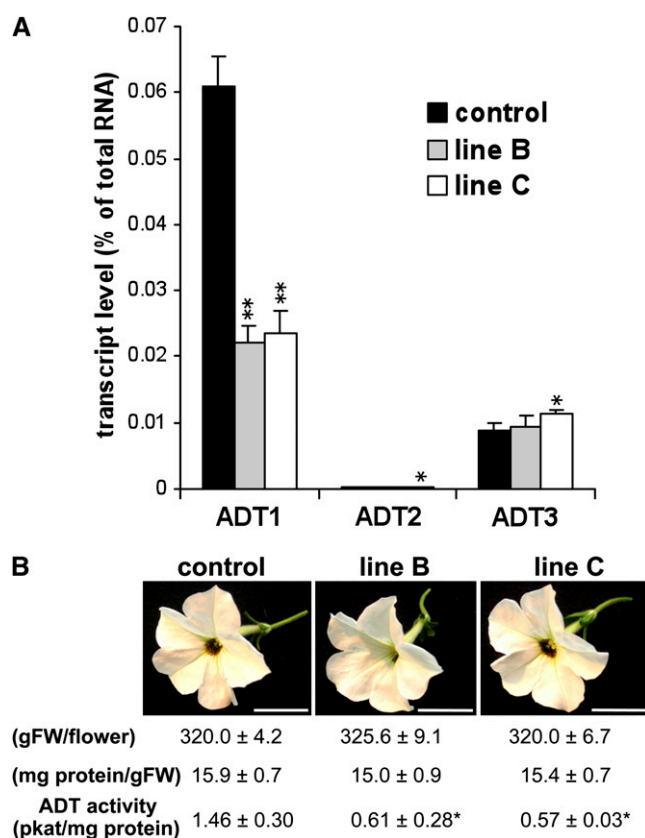


**Figure 6.** Effect of *ADT1* RNAi suppression on expression of individual *ADT* genes, flower morphology, weight, protein content, and ADT activity.

**(A)** *ADT1*, *ADT2*, and *ADT3* mRNA transcript levels determined by qRT-PCR (means ± SE,  $n = 4$  biological replicates) in the corolla of control (black bars) and transgenic B (gray bars) and C (white bars) lines harvested at 8 PM, 2 d postanthesis. \*  $P < 0.05$  and \*\*  $P < 0.01$  by Student's  $t$  test of transgenics relative to control within each gene.

**(B)** Representative 2-d postanthesis flowers of control plants and transgenic lines B and C (left to right). Flower fresh weights (gFW/flower), protein concentrations (mg protein/gFW), and ADT activity (pkat/mg protein) in petunia corollas are indicated as means ± SE ( $n = 6$  biological replicates). Bars = 2 cm.

was not significantly altered in transgenic lines (see Supplemental Table 1 online), suggesting that either salicylic acid in petunia petals is mainly produced via a Phe-independent pathway (Wildermuth et al., 2001) or that the remaining 20% of Phe in transgenic plants is sufficient to support salicylic acid production. Unexpectedly, the level of shikimic acid was significantly reduced in both transgenic lines relative to controls (by 67 to 89%; Figure 7; see Supplemental Table 1 online).

Detection of arogenate in plant tissues was formerly found to be difficult due to its low level and acid-labile property (Zamir et al., 1983; Razal et al., 1994). By combining a previously developed extraction protocol (Razal et al., 1994) with arogenate detection using liquid chromatography-mass spectrometry (LC-MS), we were able to analyze its levels in petunia petals. The identity of the peak was confirmed by comparing its reten-

tion time and mass spectra with those of an arogenate standard (see Supplemental Figure 3 online). Unexpectedly, no significant differences were observed for the arogenate levels between transgenic and control petals (Figure 7; see Supplemental Table 1 online). The levels of prephenate and phenylpyruvate were also analyzed by taking advantage of acid and alkali labile properties of prephenate and phenylpyruvate, respectively (Davis, 1953; Doy and Gibson, 1961; Zamir et al., 1983; see Methods and Supplemental Figure 4 online). While the levels of phenylpyruvate were below the detection limit ( $<0.5$  nmol/gFW), low but similar levels of prephenate were detected in petals of all genotypes (Figure 7; see Supplemental Table 1 online).

Interestingly, downregulation of *ADT1* gene expression did not alter the level of Tyr, which is also derived from arogenate by arogenate dehydrogenase (Bonner and Jensen, 1987; Figure 7; see Supplemental Table 1 online). However, the levels of Trp, which is derived from chorismate, were significantly reduced in both transgenic lines relative to controls (Figure 7; see Supplemental Table 1 online). The levels of mono- and diglycosides of quercetin and kaempferol, flavonols known to accumulate in the petals of *P. hybrida* (Griesbach and Asen, 1990; Griesbach and Kamo, 1996), remained unaltered in transgenic petals (see Supplemental Figure 5 online).

#### Downregulation of the Shikimate Pathway in *ADT1* RNAi Petals

A 67 to 89% decrease in the endogenous pool of shikimic acid in transgenic petals (Figure 7; see Supplemental Table 1 online) could be a consequence of downregulation of flux toward shikimate in *ADT1*-RNAi petunia flowers. To test this hypothesis, petals of control and transgenic line B flowers were fed with uniformly  $^{13}\text{C}$ -labeled ( $[\text{U-}^{13}\text{C}_{12}]$ ) sucrose, the major carbon source for flowers, for 6 h starting at 6 PM, when active Phe biosynthesis takes place (Figures 3B and 3D), and pool sizes and isotopic labeling of shikimate as well as sucrose at different time points were analyzed (Figure 9). In both genotypes, sucrose labeling always slightly exceeded labeling of shikimate, consistent with a simple precursor-product relationship between sucrose and shikimate (Figure 9). Over this time course, the shikimate pool was significantly reduced in transgenic petals relative to the control, while there was little difference in its isotopic labeling (Figure 9B). The sucrose labeling pattern was nearly identical in both control and transgenic petals (Figure 9A). These results together indicate that in transgenic petals the carbon flux toward shikimate is decreased in proportion to the reduced pool size of shikimate. Similar results were obtained when feeding experiments were performed for 16 h starting at 11 AM (see Supplemental Figure 6 online).

If an unaltered level of arogenate in transgenic petals is the result of a reduction in shikimate pool size, the supply of exogenous shikimate may lead to arogenate accumulation. To test this hypothesis, petunia petals were fed with 300  $\mu\text{mol}$  shikimate for 7 h starting at 3 PM, and pool sizes of arogenate, prephenate, and phenylpyruvate as well as aromatic amino acids were analyzed. Feeding of transgenic petals with shikimate resulted in nearly a fivefold increase in the level of arogenate relative to the control (Figure 10). Moreover, prephenate and

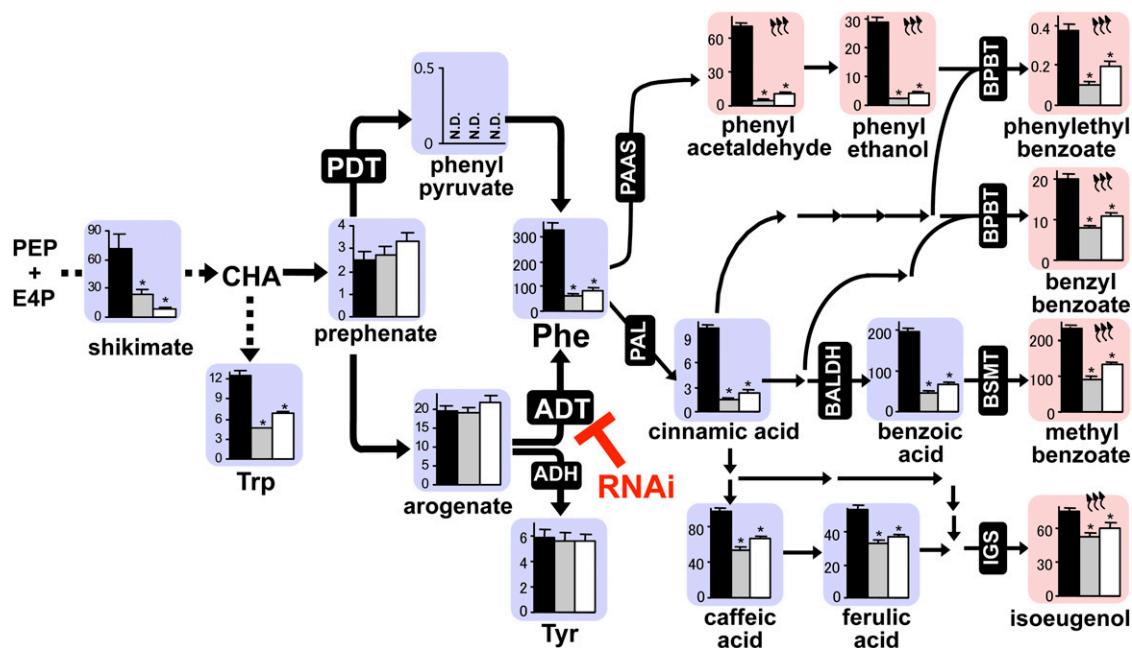


**Figure 7.** Effects of *ADT1* RNAi Suppression on Phenylpropanoid/Benzenoid Compounds, Aromatic Amino Acids, and the Shikimate Pathway Intermediates.

Schematic representation of the shikimate and Phe biosynthetic pathways and benzenoid/phenylpropanoid network in petunia petals. Metabolite levels (blue background) and volatile emission (pink background with three vertical arrows) are shown in nmol/gFW and nmol/gFW/h, respectively. Black, gray, and white bars indicate the control and transgenic lines B and C, respectively. Data are means  $\pm$  SE ( $n$  = at least 5 biological replicates). N.D., not detectable ( $<0.5$  nmol/gFW). \*  $P < 0.01$  by Student's  $t$  test of transgenics relative to control. ADH, aroclinate dehydrogenase; CHA, chorismate; E4P, erythrose 4-phosphate; PEP, phosphoenolpyruvate.

phenylpyruvate, which were previously at low or undetectable levels (Figure 7), became readily measureable in both genotypes after shikimate feeding with transgenic petals accumulating approximately threefold higher level than control (Figure 10). Shikimate feeding partially recovered the reduced levels of endogenous Phe and Trp in transgenic petals, although differences between genotypes remained significant (Figure 10). Tyr levels were similarly increased in both transgenic and control petals after shikimate feeding.

To determine whether reduced shikimate pathway flux in *ADT1*-RNAi lines (Figure 9) is the result of downregulation of expression of 3-deoxy-D-*arabino*-heptulosonate 7-phosphate synthase (DAHPS), which catalyzes the first committed step in the shikimate pathway (Bentley, 1990; Herrmann and Weaver, 1999), *DAHPS* transcript level was analyzed in petals of two transgenic petunia lines and control plants using qRT-PCR. We also analyzed expression of genes encoding enzymes of the shikimate pathway downstream of shikimate (e.g., 5-enolpyruvylshikimate 3-phosphate synthase [EPSPS] and CM) as well as ODORANT1 (ODO1), which was shown to regulate the flux through the shikimate pathway in petunia petals (Verdonk et al., 2005). Surprisingly, the reduction in *ADT1* expression in transgenic flowers led to an  $\sim 1.3$  to 1.5-fold increase in *DAHPS*, *EPSPS*, and *CM* transcript levels relative to controls, while *ODO1* expression remained unaffected in flowers of transgenic line B and were slightly decreased in line C (Figure 11).

**DISCUSSION**

**The Postchorismate Pathway(s) for Phe Biosynthesis**

Although there is no direct genetic evidence showing the actual routes responsible for Phe formation in plants, it is believed that Phe biosynthesis occurs via the aroclinate pathway based on the detection of ADT activities in a broad variety of plant crude extracts (Jung et al., 1986; Siehl and Conn, 1988) and the

**Table 2.** Activities of Enzymes Involved in Phe and Phenylpropanoid/Benzenoid Biosynthesis in Petunia Petals of Control and *ADT1*-RNAi Lines

	Control	Line B	Line C
PAAS	0.018 $\pm$ 0.002	0.016 $\pm$ 0.002	0.016 $\pm$ 0.001
BSMT	0.69 $\pm$ 0.04	0.69 $\pm$ 0.04	0.74 $\pm$ 0.16
BPBT	7.65 $\pm$ 0.55	6.37 $\pm$ 0.32	6.91 $\pm$ 0.85
IGS	0.081 $\pm$ 0.006	0.108 $\pm$ 0.023	0.098 $\pm$ 0.013
PAL	105.8 $\pm$ 9.1	100.8 $\pm$ 7.5	108.9 $\pm$ 5.9
BALDH	3.98 $\pm$ 0.42	5.27 $\pm$ 0.71	4.58 $\pm$ 1.06

Petal crude extracts were prepared from flowers harvested at 8 PM, 2 d postanthesis. Data are means  $\pm$  SE ( $n$  = 4 to 6 biological replicates) and expressed in pkat/mg protein. Activities were not significantly different between genotypes ( $P > 0.05$  by Student's  $t$  test).



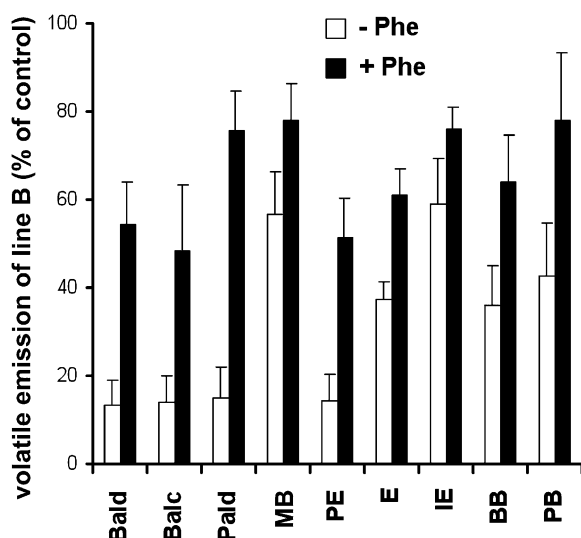


**Figure 8.** Recovery of Benzenoid and Phenylpropanoid Volatile Emission from Transgenic *ADT1*-RNAi Petunia Flowers by Feeding with Exogenous Phe.

Emitted volatiles were collected from control and transgenic petunia flowers 2 d postanthesis from 8 PM to 12 AM in the presence (open bars) and absence (closed bars) of exogenous Phe. Results are presented as a percentage of emission of individual compounds in transgenic line B relative to control flowers. Data are means  $\pm$  SE ( $n = 3$  biological replicates). Bald, benzaldehyde; Balc, benzylalcohol; BB, benzylbenzoate; E, eugenol; IE, isoeugenol; MB, methylbenzoate; Pald, phenylacetaldehyde; PB, phenylethylbenzoate; PE, 2-phenylethanol.

biochemical properties of isolated *Arabidopsis* and rice ADTs (Cho et al., 2007; Yamada et al., 2008). In this study, we were also able to detect ADT activity as well as aroenate, but not phenylpyruvate, in petunia petals (Figures 6B and 7). To obtain direct evidence of the actual route(s) responsible for Phe production in planta, we identified the ADT/PDT genes expressed in petunia flowers and genetically altered Phe biosynthesis in this particular organ. A search of all available petunia EST databases predominantly generated from flower tissues identified three cDNAs with similarity to known ADT/PDT genes (Figure 2; see Supplemental Figure 1 online), which exhibited different levels of expression in petunia petals (Figures 3C to 3E). As the petunia genome has not been sequenced, additional genes may exist that encode ADT or PDT, but their expression levels in flowers are likely very low based on their absence in petunia EST databases.

All three petunia ADT proteins were targeted to plastids (Figure 4), suggesting their potential involvement in Phe biosynthesis in this compartment. Biochemical characterization of recombinant petunia ADTs showed that all ADT enzymes can convert aroenate to Phe in vitro. The apparent  $K_m$  value of petunia ADT1 for aroenate (179  $\mu$ M) is very close to that of rice ADT (120  $\mu$ M; Yamada et al., 2008) and is 2.4-fold lower than the lowest apparent  $K_m$  value of six *Arabidopsis* ADTs ranging from 400  $\mu$ M to 10.1 mM (Cho et al., 2007), while petunia ADT2 and ADT3 have the lowest apparent  $K_m$  values for aroenate among known plant ADTs to date (66.7 and 48.8  $\mu$ M, respectively). ADT2 and ADT3 could also use prephenate as a substrate, although with catalytic

efficiencies that are 231- and 133-fold lower, respectively, than that with aroenate (Table 1). By contrast, petunia ADT1 was unable to use prephenate.

Consistent with its being represented by the highest number of ESTs, transcripts of *ADT1* were found to be the most abundant among the three ADTs in the scent-producing parts of petunia flowers (Figure 3E). *ADT1* expression was also developmentally regulated and changed over a daily light/dark cycle (Figures 3C and 3D), positively correlating with the endogenous pools of Phe in petals (Figures 3A and 3B). RNAi downregulation of *ADT1* expression resulted in a significant reduction of ADT activity and Phe levels (up to 82%) in transgenic petals (Figures 6B and 7), providing genetic evidence that ADT1 plays a major role in Phe biosynthesis in petunia petals. The remaining Phe in the *ADT1*-RNAi petals could be derived from residual ADT1 activity, dehydratase activities of ADT2 or ADT3, and/or additional ADT/PDTs, if any. Our results indicate that, in petunia petals, ADT1 activity accounts for the majority of Phe production; thus, Phe biosynthesis occurs predominantly via aroenate.

Unexpectedly, the endogenous pool of aroenate was not altered by *ADT1* suppression (Figure 7) and only shikimate feeding led to its significant expansion in transgenic *ADT1*-RNAi petals relative to controls (Figure 10). The exogenous supply of shikimate also led to an accumulation of phenylpyruvate at detectable levels in both control and transgenic petals, with the

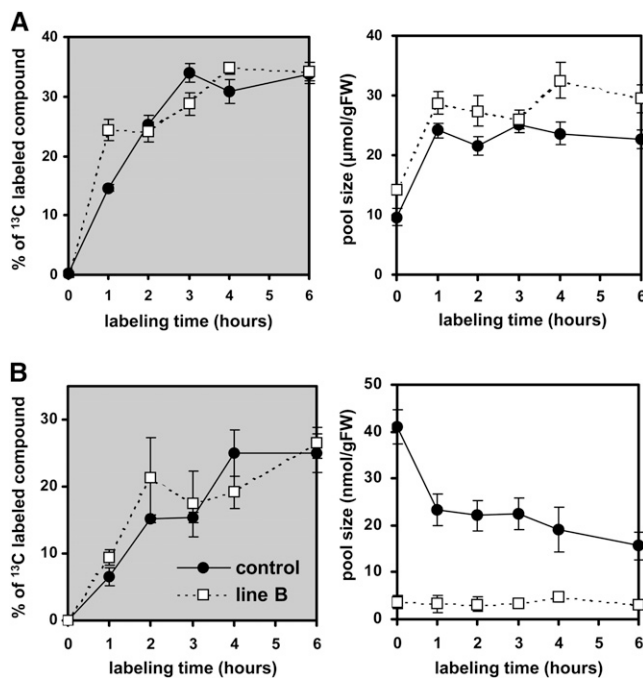


**Figure 9.** Isotopic Abundances and Pool Sizes of Shikimate in Control and *ADT1*-RNAi Petunia Petals during Feeding with  $^{13}\text{C}$ -Sucrose for 6 h.

$^{13}\text{C}$  isotopic abundances (gray panels) and pool sizes (white panels) of sucrose (A) and shikimate (B) were analyzed during a 6-h time course of [ $^{13}\text{C}_{12}$ ]-sucrose feeding to excised petals of control (solid circle) and transgenic line B (open square) plants. Data are means  $\pm$  SE ( $n = 3$  technical replicates). Similar results were obtained during a 16-h time course (see Supplemental Figure 6 online).

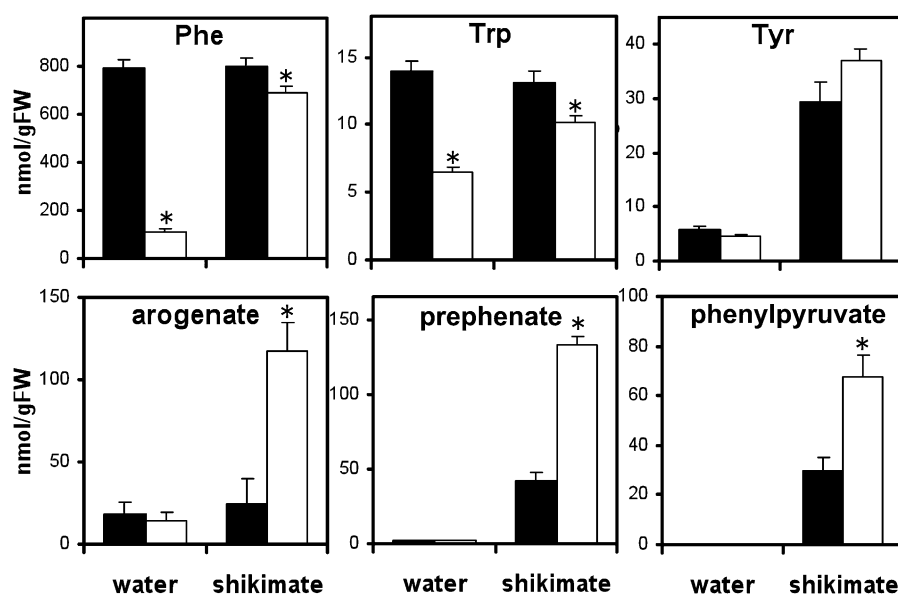


**Figure 10.** Effects of Feeding with Exogenous Shikimate on the Levels of Aromatic Amino Acids, Arogenate, Prephenate, and Phenylpyruvate in Control and *ADT1*-RNAi Petunia Petals.

Excised petals of control and transgenic line B (closed and open bars, respectively) plants were fed with water or 100 mM shikimate for 7 h (from 3 to 10 PM), and the levels of Phe, Trp, Tyr, arogenate, prephenate and phenylpyruvate were analyzed. Data are means  $\pm$  SE ( $n = 4$  biological replicates). \*  $P < 0.05$  by Student's *t* test of transgenics relative to the corresponding control.

latter accumulating higher levels (Figure 10). These results suggest that when the flux toward prephenate is increased, prephenate could also be converted to phenylpyruvate, presumably by PDT activity of ADT2, ADT3, and/or additional unidentified ADT/PDTs. The partial recovery of the reduced Phe level in the shikimate-fed transgenic petals (Figure 10) implies that phenylpyruvate can be further converted to Phe, or, alternatively, the high level of arogenate is converted to Phe via residual ADT activity (Figure 6B). However, recent heterologous overexpression of Phe-insensitive *E. coli* CM/PDT enzyme in *Arabidopsis* drastically increased Phe levels (Tzin et al., 2009), and feeding of deuterium-labeled Phe to petunia petals resulted in label incorporation into phenylpyruvate (Orlova et al., 2006), suggesting that *Arabidopsis* leaves and petunia petals contain reversible aminotransferase activity, which can interconvert phenylpyruvate and Phe (Liepman and Olsen, 2004). Taken together, these results suggest that the phenylpyruvate pathway can operate in planta; however, its contribution to Phe biosynthesis under different physiological conditions requires further investigation.

#### Role of Phe Levels in the Formation of Phenylpropanoid/benzenoid Volatiles

Phe is a precursor of numerous phenolic compounds produced in plants. However, little is known about the contribution of Phe levels to their production. An analysis of the Phe levels in petunia petals revealed a positive correlation between endogenous Phe levels and the emission of benzenoid and phenylpropanoid compounds during flower development and over daily light/dark cycles (Figures 3A and 3B; Kolosova et al., 2001; Verdonk

et al., 2003). Moreover, a drastic decrease in the level of Phe (by 75 to 82% from levels in control flowers) achieved by *ADT1* RNAi suppression resulted in up to a 70% reduction in total emission of phenylpropanoid/benzenoid compounds relative to controls (see Supplemental Table 1 online), a phenotype that could be partially rescued by feeding transgenic flowers with exogenous Phe (Figure 8). Since the activities of scent-producing enzymes (i.e., BSMT, BPBT, IGS, and PAAS) as well as PAL, which catalyzes the first entry step to the phenylpropanoid/benzenoid network, were not altered in transgenic petals (Table 2), these results suggest that the level of Phe is one of the major factors in determining the amounts of benzenoid/phenylpropanoids produced in petunia flowers.

In this study, Phe biosynthesis was reduced in petunia petal tissue without deleterious effects on plant growth and development, providing a unique opportunity to examine the impacts of altered Phe biosynthesis on phenylpropanoid/benzenoid formation. The decreased Phe levels in the *ADT1*-RNAi petals resulted in varying degrees of reduction in the emission of different phenylpropanoid/benzenoid volatiles (Figure 7; see Supplemental Table 1 online). The phenylacetaldehyde branch (which includes phenylacetaldehyde and phenylethanol) was reduced by 86 to 93%, the methylbenzoate branch (methylbenzoate, benzylalcohol, benzylacetate, and benzaldehyde) by 59 to 73%, while the isoeugenol branch (isoeugenol and eugenol) by only 21 to 32% in transgenic flowers relative to the control (Figure 7). Unaltered activities of scent-producing enzymes as well as PAL and BALDH (Table 2) suggest that branch-specific changes in enzyme levels are not responsible for different degrees of reduction in volatile emissions of individual compounds. Interestingly, the branch

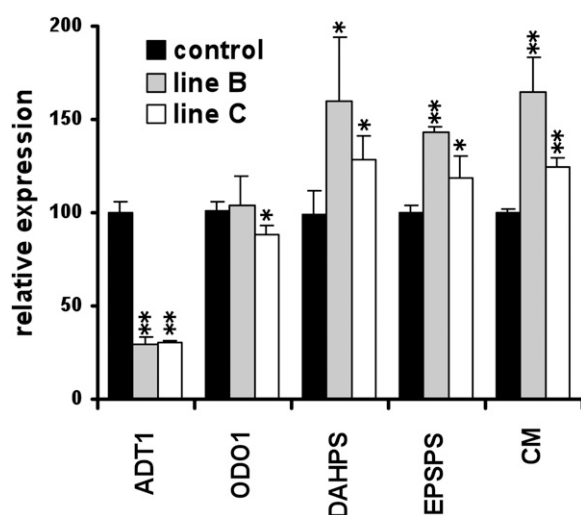


**Figure 11.** Expression Levels of Genes Encoding Shikimate Pathway Enzymes and ODO1 Transcription Factor in Control and *ADT1*-RNAi Petunia Petals.

Expression levels of *DAHPS*, *EPSPS*, and *CM* and their transcriptional activator *ODO1* were analyzed in the corolla of *ADT1*-RNAi lines B and C (gray and white bars, respectively) harvested 2 d postanthesis at 8 PM and compared with those in the control (black bars). Expression values for lines B and C were indicated as percentages of corresponding value of control petals, which is set at 100%. Data are means  $\pm$  SE ( $n = 4$  biological replicates). \*  $P < 0.05$  and \*\*  $P < 0.01$  by Student's *t* test of transgenics relative to control within each gene.

located downstream of the enzyme with the highest apparent  $K_m$  for Phe was most sensitive to reduction in Phe level. The highest reduction was observed for phenylacetaldehyde, which is synthesized by PAAS, whose  $K_m$  value (1.2 mM) is 17- to 80-fold higher than those of plant PALs (15 to 70  $\mu$ M) (Hanson and Havir, 1981; Jorin and Dixon, 1990; Appert et al., 1994; Cochrane et al., 2004; Kaminaga et al., 2006). By contrast, the least affected isoeugenol branch is located downstream of cinnamate 4-hydroxylase, which generally has a very low  $K_m$  value toward cinnamic acid, ranging in plants from 2.5 to 9  $\mu$ M (Gabriac et al., 1991; Koopmann et al., 1999; Hübner et al., 2003). Thus, at least in part, relative substrate affinities of branch point enzymes likely contribute to the differential effect of Phe reduction on phenylpropanoid/benzenoid volatile emission. Other factors, such as branch-specific Phe-independent pathway(s) (Orlova et al., 2006), metabolic channeling (Achnine et al., 2004; Winkel, 2004; Graham et al., 2007), and/or feed-forward regulation (Thomas et al., 1999; Waller et al., 2010), could also be involved in the metabolic flux redistribution upon reduced Phe levels; thus, their contribution remains to be determined. Similar differential effects on scent formation were recently observed in petunia flowers with reduced *CM* gene expression (Colquhoun et al., 2010).

#### Regulation of the Shikimate Pathway Leading to Phe Biosynthesis

Prior studies suggested that in microorganisms and plants the regulation within the postchorismate Phe pathway is similar,

whereas the flux into the shikimate pathway in plants is differently regulated than in microorganisms and poorly understood (Herrmann, 1995). Within the postchorismate pathway, Phe feedback regulates *CM* and *ADT* (or *PDT*), which in turn control the partitioning of carbon flow between the pathways leading to Phe, Tyr, and Trp in both microbes and plants (Figure 1; Gilchris et al., 1972; Jung et al., 1986; Siehl and Conn, 1988; Romero et al., 1995; Yamada et al., 2008). *DAHPS* synthase catalyzes the entry step of the shikimate pathway and in microorganisms is regulated transcriptionally and is also subjected to feedback regulation by Phe at the enzyme level (Bentley, 1990; Herrmann and Weaver, 1999). In plants, *DAHPS* synthase genes are transcriptionally regulated and induced in response to various environmental stimuli (Dyer et al., 1989; Keith et al., 1991; Görlach et al., 1995). At the enzyme level, however, all plant *DAHPS* synthases examined to date are insensitive to Phe (Huisman and Kosuge, 1974; Suzich et al., 1985; Herrmann, 1995). Thus, it is unclear whether the carbon flow into the shikimate pathway is regulated posttranscriptionally in plants.

A striking finding of this study is that transgenic *ADT1*-RNAi petals had unaltered levels of aroenate and decreased levels of shikimate and Trp (Figure 7; see Supplemental Table 1 online). The reduction in shikimate levels is unlikely due to an increased utilization of shikimate given that the levels of all three aromatic amino acids as well as phenylpropanoid/benzenoid compounds were either decreased or unchanged in transgenic plants relative to the control (Figure 7). Stable isotope labeling experiments (Figure 9) further indicate that in transgenic petals the flux toward shikimate is reduced relative to controls, resulting in an unaltered aroenate pool. Unexpectedly, the transcript levels of *DAHPS*, *EPSPS*, and *CM* were upregulated, likely to compensate for the low levels of Phe, while the expression of *ODO1*, a transcriptional activator of *DAHPS*, *EPSPS*, and *CM* (Verdonk et al., 2005), was almost unchanged in transgenic petals relative to controls (Figure 11). These results suggest that, in response to reduced Phe levels, *ADT1*-RNAi petals upregulate shikimate pathway gene expression independently of *ODO1*; however, posttranscriptional regulation overrides this transcriptional compensation and downregulates the flux through the shikimate pathway.

Currently, the nature of this posttranscriptional regulation of the shikimate pathway, which can occur at the level of translation (Wang and Sachs, 1997; Raney et al., 2002), protein modification (Huber and Huber, 1996; Savage and Ohlrogge, 1999; Tetlow et al., 2004; Uhrig et al., 2008), and/or enzyme activity (Ghosh and Preiss, 1966; Gilchris et al., 1972; Chollet et al., 1996), is unknown. Exogenously supplied shikimate clearly bypasses this negative regulation and leads to elevated accumulation of aroenate in transgenic petals (Figure 10), suggesting that the regulation occurs upstream of shikimate. In contrast with reduced shikimate levels in *ADT1*-RNAi petals, inhibition of *EPSPS*, which converts shikimate 3-phosphate to EPSP, by the herbicide glyphosate drastically increases shikimate levels in various plant species (Amrhein et al., 1980; Harring et al., 1998; Buehring et al., 2007; Henry et al., 2007). Taken together with the decreased level of Trp in transgenic petunia petals (Figure 7), it appears that a factor(s) downstream of chorismate likely serves as a regulator(s) of the flux through the shikimate pathway. In 1986, a hypothetical model was proposed for sequential

feedback regulation of Phe biosynthesis in which arogenate was viewed as a DAHP synthase feedback regulator that acts as a sensor of the overall Phe level (Jensen, 1986). Indeed, ADT from tobacco (*Nicotiana sylvestris*), spinach (*Spinacia oleracea*), *Sorghum bicolor*, and rice (Jung et al., 1986; Siehl and Conn, 1988; Yamada et al., 2008) and DAHPS from mung bean (*Vigna radiata*) and spinach (Rubin and Jensen, 1979; Doong et al., 1993) were shown to be inhibited in vitro by Phe and arogenate, respectively. Although this model still awaits genetic proof, our data are consistent with this hypothesis. Moreover, the rice *mtr1* mutant carrying Phe feedback-insensitive ADT overaccumulates Phe and Trp (Yamada et al., 2008), implying that the depletion of the arogenate pool removes this negative regulation of the shikimate pathway, leading to an overaccumulation of both Phe and Trp. However, feeding of exogenous arogenate, prephenate, or phenylpyruvate to wild-type petunia petals had little effect on the shikimate levels (see Supplemental Figure 7 online), which could be due to the inability of these pathway intermediates to reach the site of action in the plastids, as none of them has been shown to be transported across plastid membranes. Future application of metabolic control analysis (Fell, 1997; Rios-Esteva and Lange, 2007; Marshall Colón et al., 2010) may help to further define the specific biochemical step(s) that exerts the greatest control over the flux through the shikimate pathway.

In conclusion, this study provides both biochemical and genetic evidence that Phe is produced predominantly via arogenate in petunia petals. Under an elevated supply of shikimate, the phenylpyruvate route can also operate, but the negative regulation of the shikimate pathway uncovered in this study likely prevents the potential carbon overflow to the phenylpyruvate route under normal conditions. Although these studies were conducted in one model system, petunia petals, our data facilitate an in-depth understanding of the pathway and regulation of Phe biosynthesis in plants and provide useful information for rational engineering of the biosynthetic pathways leading to Phe and numerous phenolic compounds.

## METHODS

### Plant Materials and Transformation

*Petunia hybrida* cv Mitchell plants (Ball Seed Co.) were grown under standard greenhouse conditions (Dudareva et al., 2000) with a light period from 6 AM to 9 PM. For the ADT1-RNAi construct, a fragment of petunia ADT1 (444 bp in size) starting immediately after the ATG codon was subcloned into the pENTR/D-TOPO vector (Invitrogen) using the forward, 5'-CACCTGCAGTCCCTTACTCCTTCA-3', and reverse, 5'-CTTTCCAGCAGCAGCTTCG-3' primers. After verification by sequencing, LR Clonase (Invitrogen) was used to splice a 444-bp fragment into the pLISG vector, which was generated by placing gateway cloning *attR* sites from pHellsGate8 (AF489904) into the *XhoI/BclI* and *BamHI/SpeI* sites of a modified pRNA69 vector containing the LIS promoter from *Clarkia breweri* in place of the 35S promoter (Orlova et al., 2006). The section of this constructed plasmid containing the LIS promoter and gateway cloning sites in opposite orientation separated by the intron was ligated into the pART27 binary vector (Gleave, 1992) at the *SacI* and *SpeI* sites to obtain a pLISG vector. ADT1-RNAi transgenic plants were obtained via *Agrobacterium tumefaciens* (strain GV3101 carrying plasmid pLISG-ADT1-RNAi) transformation using the standard leaf disk transformation method

(Horsch et al., 1985). Rooted plants were screened for the presence of the LIS promoter by PCR with the forward, 5'-GGCACCCACTTCTTAATGATC-3' (LIS-F), and reverse, 5'-CTGGGATATGATAGGATGTGG-3' (LIS-R), primers and for the kanamycin resistance *nptII* gene using the following forward and reverse primers: 5'-TATTCGGCTATGACTGGGCA-3' (NPT-F) and 5'-GCCAACGCTATGTCCTGATA-3' (NPT-R). T0 and T1 transformants were self-pollinated manually, and the obtained seeds were analyzed for segregation by germinating on Murashige and Skoog medium supplemented with kanamycin (200 mg/L). Seeds of transgenic lines B and C showed 151:45 and 230:74 segregations for kanamycin resistance, respectively, following 3:1 segregation ( $\chi^2$  test,  $P > 0.5$ ). All analyses were conducted using T1 transformants showing kanamycin resistant as well as suppression of ADT1 gene expression.

### Phylogenetic Analysis

Phylogenetic analysis was conducted with MEGA software (version 4.02; Tamura et al., 2007). The amino acid sequences were aligned using ClustalW and then adjusted manually. Unrooted neighbor-joining trees were constructed with the following parameters: number of differences, complete deletion, and bootstrap (1000 replicates).

### RNA Isolation, RNA Gel Blot Analysis, and Quantitative Real-Time RT-PCR

For each RNA sample, at least 10 flower petals were harvested at 8 PM, 2 d after anthesis, and immediately frozen in liquid nitrogen. RNA gel blot analysis was performed as previously described (Boatright et al., 2004). Total RNA was isolated using an RNeasy plant mini kit (Qiagen), and 5  $\mu$ g of RNA was loaded in each lane. A 1.3-kb *EcoRI* fragment containing the ADT1 coding region was used as a probe for RNA gel blot analysis. The blots were rehybridized with an 18S rRNA probe as a loading control. Autoradiography was performed overnight.

For qRT-PCR, the isolated total RNA was treated with DNase I to eliminate genomic DNA using the TURBO DNA-free kit (Ambion), and 1  $\mu$ g of RNA was subsequently reverse-transcribed to cDNA in a total volume of 100  $\mu$ L using the High Capacity cDNA reverse transcription kit (Applied Biosystems). Petunia gene-specific primers, ADT1 forward 5'-TAACTGCGAAGCCATTCCTGC-3' and reverse 5'-CTCTACTGGTAGAAC-TGCGCG-3'; ADT2 forward 5'-ACGAAGTTGGGTTTGGTCAG-3' and reverse 5'-TGCCCCCTGCATCTTTTATGTT-3'; ADT3 forward 5'-CAAAATGTGAAGCTATTCCTTGTG-3' and reverse 5'-TTCGATCGGTAAAA-CAGCACG-3'; ODO1 forward 5'-ATTGCGCATGGGAATTC-3' and reverse 5'-GAAAGTGTCTTCCCAGGATGTCA-3'; DAHPS forward 5'-CAAAGCTCCGTGTGGTCTTAAA-3' and reverse 5'-TCCTGGG-TGGCTTCCTTCTT-3'; EPSPS forward 5'-CACCCACCGGAGAAAC-TAA-3' and reverse 5'-TGACGGGAACATCTGCACAA-3'; CM forward 5'-CCTGCTGTTGAAGAGGCTATCA-3' and reverse 5'-CAGGGTCAC-CTCCATTTTCTG-3'; and UBQ (ubiquitin 10) forward 5'-GTTAGATGTCTGCTGTCGATGGT-3' and reverse 5'-AGGAGCCAAATTAAGCACTTATCAA-3', were designed using PrimerExpress (Applied Biosystems). All primers showed 90 to 100% efficiency at a final concentration of 300 nM. For quantification of ADT1, ADT2, and ADT3 transcript levels, the pCR4-TOPO vectors carrying truncated petunia ADT1, ADT2, and ADT3 were digested with *EcoRI*, and the resulting fragments were purified from agarose gels using a Qiaquick gel extraction kit (Qiagen). After determining DNA concentration with the NanoDrop 1000 spectrophotometer (Thermo Scientific), purified DNA fragments were diluted from 2 ng/mL to 3.2 pg/mL and used to obtain standard curves in qRT-PCR with gene-specific primers. Individual qRT-PCR reactions contained 5  $\mu$ L of the SYBR Green PCR Master Mix (Applied Biosystems), 2  $\mu$ L of 50 times diluted cDNA and 1.5  $\mu$ L of 2  $\mu$ M forward and reverse primers. Two-step qRT-PCR amplification (40 cycles of 95°C for 3 s followed by 60°C for 30 s) was performed using the StepOn Real-Time PCR system (Applied

Biosystems). Based on the standard curves, absolute quantities of *ADT1*, *ADT2*, and *ADT3* transcripts were calculated and expressed as a percentage of the total RNA or relative to a control sample. For relative quantification of *DAPH5*, *EPSP*, *CM*, and *ODO1* transcript levels, *UBQ10* was used as a reference gene. Each data point represents an average of three to four independent biological samples.

#### Heterologous Expression and Purification of Recombinant Petunia ADTs

To obtain the full-length cDNA of *ADT2*, 5' rapid amplification of cDNA ends was performed according to the manufacturer's protocol (Invitrogen) with gene-specific (5'-GGCCTTGAAGGGGATTAGGTGAAT-3') and nested (5'-GCGTTAGAACAAGCGTAGATCGAGATA-3') primers. For functional expression, coding regions of petunia ADTs corresponding to mature proteins were obtained by PCR using the following forward primers, which introduced an *NdeI* site and a starting Met in place of Pro-52, Cys-47, and Ala-58 in *ADT1* (5'-CCATATGGCGAGTTCACACTCCGGCC-3'), *ADT2* (5'-CCATATGTCTAACGCCGAAAGCAACAGCC-3'), and *ADT3* (5'-CCATATGAGCAATAACACCGCCGG-3'), respectively. Reverse primers introduced a *BamHI* site downstream of the stop codon and were as follows: 5'-CGGATCCTCATTCATCCCTGAAGGAC-3' for *ADT1*, 5'-CGGATCCTCAAGCTATTCACATCTG-3' for *ADT2*, and 5'-CGGATCCTTAAGCATCCCTGGAAG-3' for *ADT3*. Amplified gene products were subcloned into the *NdeI*-*BamHI* site of the pET-28a vector containing an N-terminal (6xHis)-tag (Novagen). Sequencing confirmed that no errors were introduced during PCR amplifications.

Expression in *Escherichia coli* Rosetta cells, induction, harvesting, and crude extract preparation were performed as previously described (Kaminaga et al., 2006), with the exception of the lysis buffer, which contained 20 mM Na-phosphate, pH 7.8, 100 mM NaCl, and 10% glycerol. Protein purification was performed using fast protein liquid chromatography (GE Healthcare). Crude extracts were applied to the HisTrap FF column (1 mL; GE Healthcare), washed with a buffer containing 20 mM Na-phosphate, pH 7.8, 500 mM NaCl, and 0, 5, 20, and 40 mM imidazole, and the His-tagged protein was eluted with the same buffer containing 500 mM imidazole. The eluted fraction (1 mL) with the highest ADT activity was desalted on the Sephadex G-50 Fine column (GE Healthcare) into a buffer containing 20 mM Tris-HCl, pH 8.0, 1 mM EDTA, and 10% glycerol. Protein purity was determined by densitometry of SDS-PAGE gels after Coomassie Brilliant Blue staining and was 57.5, 42.8, and 34.8% for petunia *ADT1*, *ADT2*, and *ADT3*, respectively. The purity of the enzymes was taken into account for the determination of their respective  $k_{cat}$  values. Protein concentration was determined using the Bradford method (Bradford, 1976).

#### Enzyme Assays

ADT activity was measured according to Fischer and Jensen (1987) with some modifications. The reaction mixtures (20  $\mu$ L) contained 250 mM Na-phosphate buffer, pH 8.2, 1 mM EDTA, and 150  $\mu$ M aroenate, which was obtained by enzymatic conversion of prephenate to aroenate as previously described (Rippert and Matringe, 2002), followed by purification using ion exchange chromatography (Connelly and Siehl, 1987). After preincubation at 37°C for 5 min, 1  $\mu$ g of enzyme was added. The reaction was incubated at 37°C for 30 min before termination by 10  $\mu$ L of methanol. After centrifugation, 20  $\mu$ L of the mixture was derivatized with *o*-phthalaldehyde (Connelly and Siehl, 1987) and analyzed by HPLC using the Luna C18 (2) column (3  $\mu$ m, 100Å, 150  $\times$  4.6 mm; Phenomenex) with a 30-min linear gradient of 10 to 70% methanol in 20 mM Na-phosphate buffer, pH 6.8. The production was monitored at 336 nm and quantified based on a standard calibration curve generated with authentic Phe (Fluka). For ADT activity in petal extracts, 2 g of petal tissues

harvested at 8 PM 2 d after anthesis were ground in 7 mL of lysis buffer (20 mM Tris-HCl, pH 8.0, 1 mM EDTA, 1 mM DTT, 10% glycerol, 1 mM phenylmethylsulfonyl fluoride, 35  $\mu$ g leupeptin, and 35  $\mu$ L of protease inhibitor cocktail [Sigma-Aldrich]) and subjected to 20 to 40% ammonium sulfate precipitation (Jung et al., 1986). After desalting with a Sephadex G-50 column (GE Healthcare) and concentrating using a Amicon Ultra-4 (Millipore) to 200  $\mu$ L, 5  $\mu$ L of the protein extract was added to the total volume of the 12- $\mu$ L reaction mixture containing 500  $\mu$ M aroenate and 20 mM Tris, pH 8.0, and the mixture was incubated at 37°C for 15 min. ADT activity was expressed as pkat per mg total protein in the ammonium sulfate precipitated extract.

CM and PDT activities were determined according to Cotton and Gibson (1965), with some modifications. The reaction mixture (50  $\mu$ L) containing 20 mM Tris-HCl, pH 8.0, 1 mM EDTA, and 500  $\mu$ M chorismate or prephenate was preincubated at 37°C for 5 min. After adding 1.8 to 3  $\mu$ g of purified enzymes or 33  $\mu$ g of proteins from *E. coli* crude extracts, reaction mixtures were incubated at 37°C for 30 and 20 min for PDT and CM activities, respectively. In the case of PDT activity, the reaction was stopped with 200  $\mu$ L of 2.5 N NaOH, while the CM reaction was stopped with 50  $\mu$ L of 1 N HCl followed by 20 min of incubation at 37°C and a subsequent addition of 150  $\mu$ L 2.5 N NaOH. After centrifugation, phenylpyruvate formation was monitored spectrophotometrically at 320 nm. The identity of the phenylpyruvate product was also confirmed using HPLC and an authentic standard (Sigma-Aldrich). For HPLC analysis, the reaction was stopped with 30  $\mu$ L of methanol and 10  $\mu$ L was analyzed on an Agilent 1200 HPLC system using the Luna C18 (2) column (3  $\mu$ m, 100Å, 150  $\times$  4.6 mm; Phenomenex) at a flow rate of 1 mL/min with a 40-min linear gradient of 0 to 30% methanol in 20 mM Na-phosphate buffer, pH 6.8.

For PAL, BSMT, BPBT, PAAS, IGS, and BALDH activity, crude protein extracts were prepared from petunia petals of control and transgenic plants harvested at 8 PM, 2 d after anthesis, as described previously (Dudareva et al., 2000; Kolosova et al., 2001; Boatright et al., 2004; Kaminaga et al., 2006; Koeduka et al., 2008). PAL activity was determined by measuring the formation of U-<sup>14</sup>C-cinnamic acid from U-<sup>14</sup>C-L-Phe (Kolosova et al., 2001), and BSMT was determined by measuring the transfer of the <sup>14</sup>C-labeled methyl group of S-adenosyl-L-methionine to the carboxyl group of benzoic acid (Dudareva et al., 2000). PAAS (Kaminaga et al., 2006) and BPBT (Boatright et al., 2004) activities were determined by measuring the respective formation of phenylacetaldehyde from Phe, and benzylbenzoate from benzoyl-CoA and benzylalcohol using gas chromatography (GC)-MS. For IGS and BALDH activities, crude extracts were desalted on small Sephadex G-25 spin columns (NAP-5 column; GE Healthcare) into 50 mM Na-phosphate, pH 7.5, 1 mM DTT, and 25% glycerol for analysis of BALDH activity and 50 mM bis-Tris-HCl, pH 7.0, 10 mM  $\beta$ -mercaptoethanol, and 10% glycerol for IGS activity. BALDH and IGS activities were analyzed as described previously (Koeduka et al., 2008), with the exception that the IGS reaction was coupled with the CFAT reaction to produce coniferyl acetate (Dexter et al., 2007), a substrate for IGS.

All enzyme assays were performed at an appropriate enzyme concentration so that reaction velocity was proportional to enzyme concentration and linear during the incubation time period. Kinetic data were evaluated by hyperbolic regression analysis (HYPER.EXE, version 1.00). Triplicate assays were performed for all data points for kinetic analysis.

#### Subcellular Localization of ADT Proteins

The open reading frames and the first 80, 75, and 79 amino acids of *ADT1*, *ADT2*, and *ADT3*, respectively, were fused upstream of, and in frame with, GFP in the *XbaI* and *BamHI* cloning sites of the p326-SGFP vector containing the cauliflower mosaic virus 35S promoter (a gift from I. Hwang Pohang, University of Science and Technology, Korea). For the two *ADT1* constructs, the same forward primer, 5'-GTCTAGAATGCAGTCCCTTACTCCTTC-3', was used in combination with the following reverse

primers: 5'-CGGATCCTTCATCCCTAGAAGGACAGC-3' (for p326-PhADT1-SGFP) or 5'-CGGATCCTGAGACTACTTTGCTTGCTAAT-3' (for p326-TP<sub>1-80</sub> PhADT1-SGFP). For the two ADT2 constructs, the same forward primer, 5'-GTCTAGAAATGGCAGCCACCACTACAC-3', was used in combination with 5'-CGGATCCAGCTATTCCACTATCTGACGG-3' (for p326-PhADT2-SGFP) or 5'-CGGATCCATGTTTCATCACTGACTTTTAAAG-3' (for p326-TP<sub>1-75</sub> PhADT2-SGFP) reverse primers. For the two ADT3 constructs, the same forward primer, 5'-GTCTAGAATGCAGTCCCTTACTCCA-3', was used with two reverse primers, 5'-CGGATCCAGCATCCCTGGAAGGA-3' (for p326-PhADT3-SGFP) and 5'-CGGATCCAATTGCACACGAAGCTCTG-3' (for p326-TP<sub>1-79</sub> PhADT3-SGFP). Sequencing confirmed the accuracy of the fusions. *Arabidopsis thaliana* protoplasts were prepared and transformed as described (Sheen, 2002; Nagegowda et al., 2008). The plasmids p326-SGFP and p326-RbTP-SGFP, containing a plastidial Rubisco target peptide, were used as markers for cytosolic and plastidial localization, respectively. Transient expression of GFP fusion proteins was observed 16 to 20 h after transformation. Images were acquired using a Radiance 2100 MP Rainbow (Bio-Rad) on a TE2000 (Nikon) inverted microscope using a  $\times 60$  oil 1.4-numerical aperture lens. GFP was excited with the 488-nm line of the four-line argon, and the emission was collected with a 500LP, 540SP filter combination. Chlorophyll fluorescence was excited by the 637-nm red diode laser, and emission  $>660$  nm was collected.

#### Analysis of Floral Volatiles and Organic and Amino Acids

Floral volatiles were collected using a closed-loop stripping method (Orlova et al., 2006) from 8 PM until 8 AM using control and *ADT1*-RNAi petunia flowers (three flowers per biological replicate) harvested 2 d after anthesis. For feeding experiments, excised corolla tissues harvested 2 d after anthesis (eight petals per biological replicate) were placed on moist round filter paper (9 cm in diameter) supplied with 300  $\mu$ mol of Phe or shikimate dissolved in 3 mL of water, and volatiles were collected from 8 PM to 12 AM for Phe feedings and from 3 to 10 PM for shikimate feedings. Trapped scent compounds were eluted from Paropak Q traps (8/100 mesh size; Alltech Associates) with 300  $\mu$ L dichloromethane containing a naphthalene (200  $\mu$ g/mL) as an internal standard and analyzed by GC-MS (5975 inert XL EI/CI mass spectrometer detector combined with 6890N GC; Agilent Technologies) and an Agilent 19091S-433 HP-5MS capillary column (30 m  $\times$  0.25 mm; film thickness 0.25  $\mu$ m). Injector temperature and volume were 250°C and 1  $\mu$ L (splitless), respectively. Column temperature was held at 40°C for 3 min and then heated to 220°C at 8°C min<sup>-1</sup>. Electron ionization energy was set at 70 eV. Mass spectra were obtained in scan mode scanning across 50 to 550 atomic mass units. All volatile compounds were identified by comparing their retention times and mass spectra with those of corresponding authentic compounds. Quantification was performed using calibration curves generated from individual authentic standards (Sigma-Aldrich).

To determine the internal pools of volatiles, amino acids, and organic acids, 1 g of transgenic and control corolla tissues from at least eight flowers per sample was collected at 8 PM on the second day after anthesis to minimize the effect of rhythmicity. Internal pools of volatiles were extracted overnight by shaking the ground tissues with 10 mL of dichloromethane containing a naphthalene internal standard (200  $\mu$ g/mL), concentrated (Goodwin et al., 2003), and analyzed by GC-MS as described above. Analyses of organic and amino acids, with the exceptions of shikimate, arogenate, phenylpyruvate, and Trp, were performed as described previously (Orlova et al., 2006), with some modifications. Frozen tissue (0.5 g) was extracted overnight at 4°C with 10 mL of 100% methanol containing 250 nmol of  $\alpha$ -aminoadipic acid and 4-chlorobenzoic acid as internal standards. The extracts were mixed with 5 mL chloroform and 6 mL water for phase separation, and the resulting aqueous layer was removed, dried, and then redissolved in 4 mL of water. For organic acid analysis, 3 mL of the extract in water was mixed with 20  $\mu$ L of 1 N HCl

and extracted twice with 3 mL of ethyl acetate, which was dried and derivatized with 250  $\mu$ L of *N,O*-Bis(trimethylsilyl)trifluoroacetamide (Supelco) and 20  $\mu$ L of pyridine at 75°C for 2 h. Samples were then analyzed by GC-MS as described above, with some differences. The injector temperature was 260°C. The column temperature was held at 35°C for 3 min and then heated to 260°C at 8°C min<sup>-1</sup>. All organic acids were identified by comparing their retention times and mass spectra with those of corresponding authentic compounds. Quantification was performed using calibration curves generated from individual authentic standards.

For the amino acid analysis, 1 mL of the remaining extract was subjected to ion exchange chromatography using a Dowex 50-H<sup>+</sup>  $\times$  8, 200 mesh column (Sigma-Aldrich). Amino acids were eluted from the column with 6 mL of 6 M NH<sub>4</sub>OH, dried, dissolved in 0.4 mL of 60% methanol, and dried again. The dried sample was derivatized with 200  $\mu$ L of a 5:1 (v/v) isobutanol:acetyl chloride mixture at 120°C for 20 min, dried, derivatized again with 100  $\mu$ L of heptafluorobutyric anhydride (Sigma-Aldrich) at 120°C for 10 min, dried to incipient dryness, dissolved in 200  $\mu$ L of a 1:1 (v/v) ethyl acetate:acetic anhydride mixture, and analyzed by GC-MS as described previously (Boatright et al., 2004). All amino acids were identified by comparing their retention times and mass spectra with those of corresponding authentic compounds. Quantification was performed using calibration curves generated from an authentic mixture containing individual amino acids (Sigma-Aldrich).

Trp and flavonol extraction was performed overnight at 4°C by adding 1.8 mL of 80% methanol containing an internal standard, Leu-Leu-Leu tripeptides (14 pmol; Sigma-Aldrich), to 300 mg of petal tissue. After sonication for 20 min followed by centrifugation, the supernatant was removed and combined with 500  $\mu$ L chloroform and 200  $\mu$ L water. After phase separation, the resulting methanol/water phase was dried using vacuum centrifugation, resuspended in 100  $\mu$ L of a HPLC diluent of 5% acetonitrile containing 0.1% formic acid, and analyzed by LC-MS. Chromatographic separations were performed using an Agilent 1100 HPLC system and an Atlantis T3 (2.1  $\times$  150 mm  $\times$  3  $\mu$ m) separation column (Waters). Mobile phases were (A) 0.1% formic acid (v/v) in Milli-Q water and (B) 0.1% formic acid (v/v) in acetonitrile. After 5  $\mu$ L of sample injection, 5% B was held for 1 min, followed by a linear gradient to 75% B over 49 min and a 10-min equilibration back to 5% B at a 0.3-mL/min flow rate and 40°C column temperature. The column effluent was then introduced by positive electrospray ionization (ESI) into an Agilent 6210 MSD time-of-flight mass spectrometer. The ESI capillary voltage was 3.0 kV, nitrogen gas temperature was set to 350°C, drying gas flow rate was 11.0 L/min, nebulizer gas pressure was 30 psig, fragmentor voltage was 130 V, skimmer was 65 V, and OCT RF was 250 V. Mass data (from mass-to-charge ratios [*m/z*] of 70 to 1500) were collected and analyzed using Agilent MassHunter B.02 software. Identification and quantification of Trp were based on standard calibration curves generated from an authentic Trp standard (Sigma-Aldrich). Using the same LC-MS chromatograms, quercetin-3-*O*-glucoside and kaempferol-3-*O*-glucoside were identified by comparing their retention times, UV spectra, as well as mass spectra in positive and negative modes with those of authentic standards. The quercetin-3-*O*-glucoside and kaempferol-3-*O*-glucoside as well as the remaining two compounds detected in petunia petals had fragments of 303.05 and 287.06 *m/z* in positive mode, which correspond to the molecular ions of quercetin and kaempferol, respectively. In addition, all four flavonols had fragments of *m/z* 162.05 or 324.11 higher than the molecular ions of quercetin or kaempferol in positive mode, consistent with them being mono- or diglycosides, respectively. Relative quantification of flavonols between transgenic and control petals were conducted by extracting specific ions, *m/z* 303.05, 465.10, and 627.16, for quercetin diglycoside, 287.06, 449.11, and 611.16 for kaempferol diglycoside, 303.05 and 465.10 for quercetin-3-*O*-glucoside, and 287.06 and 449.12 for kaempferol-3-*O*-glucoside (see Supplemental Figure 5 online).



Because shikimic acid was poorly extracted by ethyl acetate during organic acid analysis, a different method was used for its extraction and analysis (Becerril et al., 1989; Singh and Shaner, 1998). Half a gram of frozen tissue was ground in liquid N<sub>2</sub> and homogenized in 1 mL of 0.25 N HCl. After centrifugation, the supernatant was filtered through a 0.45- $\mu$ m GH Polypro (GHP) filter (Pall Corporation) and analyzed by HPLC using an Agilent ZORBAX SB-C18 column (4.6  $\times$  150 mm  $\times$  3.5  $\mu$ m) with an isocratic elution of 0.1% formic acid (v/v) in Milli-Q water at a 0.5-mL/min flow rate. Shikimic acid was monitored at 215 nm and quantified based on a standard calibration curve generated with authentic shikimic acid (Sigma-Aldrich).

For the analyses of arogenate, 0.5 g tissue was ground in liquid N<sub>2</sub> and homogenized in 1.5 mL of 75% ethanol containing 0.5% 2-amino-2-methyl-1-propanol HCl, pH 11 (Razal et al., 1994), and 100 nmol of  $\alpha$ -aminoadipic acid as an internal standard. After centrifugation, 200  $\mu$ L of the supernatant was filtered through an Ultrafree-MC filter (Ultra-4; Millipore Amicon), vacuum dried, and dissolved in 50  $\mu$ L water. For arogenate analysis, 20  $\mu$ L of the sample was derivatized with *o*-phthalaldehyde and injected into LC-MS. Chromatographic separations were performed using an Agilent 1100 HPLC system and a Luna C18 (2) column (3  $\mu$ m, 100  $\text{\AA}$ , 250  $\times$  4.6 mm; Phenomenex) with a 48-min linear gradient of 10 to 70% methanol in 0.1% ammonium acetate (v/v) at a 0.3-mL/min flow rate and 35°C column temperature. The column effluent was then introduced by negative ESI into an Agilent 6210 MSD time-of-flight mass spectrometer. The ESI capillary voltage was 3.2 kV, nitrogen gas temperature was set to 350°C, drying gas flow rate was 8.0 L/min, nebulizer gas pressure was 35 psig, fragmentor voltage was 140 V, skimmer was 60 V, and OCT RF was 250 V. The arogenate peak was identified by comparing the retention time and mass spectrum of the purified arogenate standard (see above and Supplemental Figure 3 online). Quantification was based on a calibration curve generated by the authentic standard.

Poor retention of prephenate on the C18 LC column and its instability during derivatization prevented its direct analysis on LC or GC-MS. Thus, prephenate was quantified after its acid conversion to phenylpyruvate, which is readily detectable by LC-MS and degraded under alkaline conditions (Davis, 1953; Doy and Gibson, 1961; Zamir et al., 1983). Petunia petal tissue extracts were prepared as described for arogenate analysis with the exceptions of using 4-chlorobenzoic acid as an internal standard and the buffer pH of either 6 or 9. A phenylpyruvate peak detected in the petal extracts prepared at pH 6.0 represents a sum of endogenous phenylpyruvate as well as phenylpyruvate produced by acid conversion of prephenate during extraction. By contrast, extraction of petal tissues at pH 9.0 leads to degradation of endogenous phenylpyruvate under alkaline conditions (Doy and Gibson, 1961; see Supplemental Figure 4 online). However, subsequent acidification of the pH 9.0 petal extract by 0.25 N HCl treatment for 60 min at room temperature resulted in complete conversion of endogenous prephenate to phenylpyruvate (Davis, 1953; see Supplemental Figure 4 online). The difference between phenylpyruvate levels in the petal extracts prepared at pH 6.0 and 9, the latter treated with HCl, represents endogenous phenylpyruvate content. Authentic prephenate and phenylpyruvate standards added before extraction were quantitatively recovered during this procedure. Ten microliters of the sample was injected to an Agilent 1100 HPLC system and separated by an Atlantis T3 (2.1  $\times$  150 mm  $\times$  3  $\mu$ m) separation column (Waters) with a 5-min isocratic elution with 0% methanol followed by an 18-min linear gradient of 0 to 26% methanol in 0.1% ammonium acetate (v/v) at a 0.3-mL/min flow rate and 35°C column temperature. MS analysis was conducted as described for arogenate analysis with the exception of a drying gas flow rate of 9.0 L/min. The phenylpyruvate peak was identified by comparing the retention times and mass spectra of the authentic phenylpyruvate standard (see Supplemental Figure 4 online). Quantification was performed based on a calibration curve generated from the authentic standard.

### Stable Isotope Labeling of Shikimate by Feeding <sup>13</sup>C-Sucrose

Excised corolla tissues harvested 2 d after anthesis (eight petals per each biological replicate) were placed on a piece of round filter paper (4 cm in diameter; Boatright et al., 2004; Orlova et al., 2006) moistened with 500  $\mu$ L of 3% [<sup>13</sup>C<sub>12</sub>]-sucrose (Omicron Biochemicals) for a duration of 6 or 16 h and harvested in liquid N<sub>2</sub> at different time points. Shikimate was extracted from 100 mg of the frozen tissues and separated by HPLC as described above. The column effluent was then introduced by negative ESI into an Agilent 6210 MSD time-of-flight mass spectrometer. The ESI capillary voltage was 3.2 kV, nitrogen gas temperature was set to 350°C, drying gas flow rate was 10.0 L/min, nebulizer gas pressure was 50 psig, fragmentor voltage was 140 V, skimmer was 60 V, and OCT RF was 250 V. Mass data (from m/z 70 to 1000) were collected and analyzed using Agilent MassHunter B.02 software. Due to an interference of a 175.027 m/z fragment from an unknown adjacent peak, the intensity of M+2 species of shikimate (175.058 m/z) was estimated as an average of M+1 (174.053 m/z) and M+3 (176.065 m/z) species. The percentage of labeling was determined as the intensity of the shifted shikimate molecular ion divided by the sum of intensities for unshifted and shifted molecular ions after correcting for natural isotope abundance.

Sucrose was extracted from fed petal tissues and analyzed as previously described (Roessner et al., 2001), with some modifications. The frozen tissues (100 mg) were extracted in 500  $\mu$ L of methanol containing 0.5 mg of an internal standard, ribitol (Sigma-Aldrich), by incubating at 70°C for 15 min. After cooling, 500  $\mu$ L of water was added, the mixture was vortexed for 15 min and then centrifuged. Twenty microliters of the supernatant was dried and derivatized with 50  $\mu$ L of 20 mg/mL methoxyamine hydrochloride (Sigma-Aldrich) dissolved in pyridine (Thermo Scientific) for 30 min at 30°C followed by derivatization with 50  $\mu$ L of MSTFA (Sigma-Aldrich) for 90 min at 37°C. One-microliter aliquots of the derivatized solutions were injected at a split ratio of 1:4 into a GC-MS (Agilent Technologies) as described above, with the following changes: the injector temperature was 230°C and column temperature was held at 150°C for 1 min and then increased at 5°C min<sup>-1</sup> to 175°C, 1°C min<sup>-1</sup> to 185°C, and 10°C min<sup>-1</sup> to 250°C. The mass data were analyzed by Wsearch32 Ver. 1.6. (RMIT Chemistry), and the percentage of labeling was calculated as described above for shikimate.

### Accession Numbers

The GenBank/EMBL accession numbers for the sequences mentioned in this article are as follows: At ADT1, NP\_172644; At ADT2, NP\_187420; At ADT3, NP\_180350; At ADT4, NP\_190058; At ADT5, NP\_197655; At ADT6, NP\_563809; Ec PDT, BAA16484; Os ADT, AAP54696; It PDT, AAS79603; Ph ADT1, FJ790412; Ph ADT2, FJ790413; Ph ADT3, FJ790414; Sd PDT, AAT39307; and Sy PDT, NP\_440143

### Supplemental Data

The following materials are available in the online version of this article.

**Supplemental Figure 1.** Sequence Alignment of Predicted Amino Acid Sequences of Petunia ADTs with Plant and Bacterial ADT/PDTs.

**Supplemental Figure 2.** CM and PDT Activities during Purification of Petunia ADTs.

**Supplemental Figure 3.** Arogenate Detection in Petunia Petal Tissues using LC-MS.

**Supplemental Figure 4.** Flavonol Levels in Petunia Petals of Control and ADT1-RNAi Lines.

**Supplemental Figure 5.** Prephenate and Phenylpyruvate Detection in Petunia Petal Tissues Using LC-MS.

**Supplemental Figure 6.** Isotopic Abundances and Pool Sizes of Shikimate in Control and *ADT1*-RNAi Petunia Petals during Feeding with  $^{13}\text{C}$ -Sucrose for 16 h.

**Supplemental Figure 7.** Effects of Arogenate, Prephenate, and Phenylpyruvate Feeding on the Levels of Shikimate in Petunia Petals.

**Supplemental Table 1.** Volatile and Metabolite Analysis in the Petunia Petals of Control and *ADT1*-RNAi Lines B and C.

**Supplemental Data Set 1.** Protein Sequences Used to Generate the Phylogeny Presented in Figure 2.

## ACKNOWLEDGMENTS

We thank Jiameng Zheng and Christine Kish for technical assistance in the qRT-PCR experiments, Yasuhisa Kaminaga for initial help with protein purification, Jennifer Sturgis for confocal microscopy assistance, Dinesh Nagegowda for help with subcellular localization studies, Joëlle Mühlemann for help with sucrose analysis, and Joseph Ogas and Nicholas Bonawitz for critical reading of the manuscript. This work was supported by grants from the National Science Foundation (MCB-0615700 to N.D. and MCB-0718152 to E.P.) and the Fred Gloeckner Foundation (to N.D.). H.M. was supported in part by JSPS Postdoctoral Fellowship for Research Abroad (Japan Society for the Promotion of Science). A.K.S. was supported by Department of Biotechnology, Government of India.

Received December 2, 2009; revised February 11, 2010; accepted February 23, 2010; published March 9, 2010.

## REFERENCES

- Achnine, L., Blancaflor, E.B., Rasmussen, S., and Dixon, R.A. (2004). Colocalization of L-phenylalanine ammonia-lyase and cinnamate 4-hydroxylase for metabolic channeling in phenylpropanoid biosynthesis. *Plant Cell* **16**: 3098–3109.
- Amrhein, N., Deus, B., Gehrke, P., and Steinrücken, H.C. (1980). The site of the inhibition of the shikimate pathway by glyphosate. II. Interference of glyphosate with chorismate formation in vivo and in vitro. *Plant Physiol.* **66**: 830–834.
- Appert, C., Logemann, E., Hahlbrock, K., Schmid, J., and Amrhein, N. (1994). Structural and catalytic properties of the four phenylalanine ammonia-lyase isoenzymes from parsley (*Petroselinum crispum* Nym.). *Eur. J. Biochem.* **225**: 491–499.
- Becerril, J., Duke, S., and Lydon, J. (1989). Glyphosate effects on shikimate pathway products in leaves and flowers of velvetleaf. *Phytochemistry* **28**: 695–699.
- Bentley, R. (1990). The shikimate pathway - A metabolic tree with many branches. *Crit. Rev. Biochem. Mol. Biol.* **25**: 307–384.
- Boatright, J., Negre, F., Chen, X.L., Kish, C.M., Wood, B., Peel, G., Orlova, I., Gang, D., Rhodes, D., and Dudareva, N. (2004). Understanding *in vivo* benzenoid metabolism in petunia petal tissue. *Plant Physiol.* **135**: 1993–2011.
- Bonner, C., and Jensen, R. (1987). Arogenate dehydrogenase. *Methods Enzymol.* **142**: 488–494.
- Bradford, M.M. (1976). Rapid and sensitive method for quantitation of microgram quantities of protein utilizing principle of protein-dye binding. *Anal. Biochem.* **72**: 248–254.
- Buehring, N.W., Massey, J.H., and Reynolds, D.B. (2007). Shikimic acid accumulation in field-grown corn (*Zea mays*) following simulated glyphosate drift. *J. Agric. Food Chem.* **55**: 819–824.
- Byng, G.S., Whitaker, R.J., Shapiro, C.L., and Jensen, R.A. (1981). The aromatic amino acid pathway branches at L-arogenate in *Euglena gracilis*. *Mol. Cell. Biol.* **1**: 426–438.
- Catinot, J., Buchala, A., Abou-Mansour, E., and Metraux, J.P. (2008). Salicylic acid production in response to biotic and abiotic stress depends on isochorismate in *Nicotiana benthamiana*. *FEBS Lett.* **582**: 473–478.
- Cho, M.H., et al. (2007). Phenylalanine biosynthesis in *Arabidopsis thaliana* - Identification and characterization of arogenate dehydratases. *J. Biol. Chem.* **282**: 30827–30835.
- Chollet, R., Vidal, J., and Oleary, M.H. (1996). Phosphoenolpyruvate carboxylase: A ubiquitous, highly regulated enzyme in plants. *Annu. Rev. Plant Physiol.* **47**: 273–298.
- Cochrane, F.C., Davin, L.B., and Lewis, N.G. (2004). The Arabidopsis phenylalanine ammonia lyase gene family: Kinetic characterization of the four PAL isoforms. *Phytochemistry* **65**: 1557–1564.
- Connelly, J.A., and Siehl, D.L. (1987). Purification of chorismate, prephenate, and arogenate by HPLC. *Methods Enzymol.* **142**: 422–431.
- Colquhoun, T.A., Schimmel, B.C., Kim, J.Y., Reinhardt, D., Cline, K., and Clark, D.G. (2010). A petunia chorismate mutase specialized for the production of floral volatiles. *Plant J.* **61**: 145–155.
- Cotton, R.G.H., and Gibson, F. (1965). Biosynthesis of phenylalanine and tyrosine - Enzymes converting chorismic acid into prephenic acid and their relationships to prephenate dehydratase and prephenate dehydrogenase. *Biochim. Biophys. Acta* **100**: 76–88.
- Croteau, R., Kutchan, T.M., and Lewis, N.G. (2000). Natural products (secondary metabolites). In *Biochemistry and Molecular Biology of Plants*, R.B. Buchanan, W. Gruissem, and R. Jones, eds (Rockville, MD: American Society of Plant Physiology), pp. 1250–1318.
- Cseke, L., Dudareva, N., and Pichersky, E. (1998). Structure and evolution of linalool synthase. *Mol. Biol. Evol.* **15**: 1491–1498.
- Davidson, B.E., Blackburn, E.H., and Doppeide, T.A. (1972). Chorismate mutase-prephenate dehydratase from *Escherichia coli* K-12. 1. Purification, molecular weight, and amino acid composition. *J. Biol. Chem.* **247**: 4441–4446.
- Davis, B.D. (1953). Autocatalytic growth of a mutant due to accumulation of an unstable phenylalanine precursor. *Science* **118**: 251–252.
- Dexter, R., Qualley, A., Kish, C.M., Ma, C.J., Koeduka, T., Nagegowda, D.A., Dudareva, N., Pichersky, E., and Clark, D. (2007). Characterization of a petunia acetyltransferase involved in the biosynthesis of the floral volatile isoeugenol. *Plant J.* **49**: 265–275.
- Doong, R.L., Ganson, R.J., and Jensen, R.A. (1993). Plastid-localized 3-deoxy-D-arabino-heptulosonate 7-phosphate synthase (DS Mn): The early-pathway target of sequential feedback inhibition in higher plants. *Plant Cell Environ.* **16**: 393–402.
- Doy, C.H., and Gibson, F. (1961). The formation of 4-hydroxyphenylpyruvic acid and phenylpyruvic acid by tryptophan auxotrophs and wild-type *Aerobacter aerogenes* considered in relation to the general aromatic pathway. *Biochim. Biophys. Acta* **50**: 495–505.
- Dudareva, N., Murfitt, L.M., Mann, C.J., Gorenstein, N., Kolosova, N., Kish, C.M., Bonham, C., and Wood, K. (2000). Developmental regulation of methyl benzoate biosynthesis and emission in snapdragon flowers. *Plant Cell* **12**: 949–961.
- Dyer, W., Henstrand, J., Handa, A., and Herrmann, K. (1989). Wounding induces the first enzyme of the shikimate pathway in Solanaceae. *Proc. Natl. Acad. Sci. USA* **86**: 7370–7373.
- Fell, D. (1997). Understanding the Control of Metabolism. (London: Portland Press).
- Fischer, R., and Jensen, R. (1987). Arogenate dehydratase. *Methods Enzymol.* **142**: 495–502.
- Gabriel, B., Werckreichhart, D., Teutsch, H., and Durst, F. (1991). Purification and Immunocharacterization of a plant cytochrome P450: the cinnamic acid 4-hydroxylase. *Arch. Biochem. Biophys.* **288**: 302–309.

- Ghosh, H.P., and Preiss, J. (1966). Adenosine diphosphate glucose pyrophosphorylase: A regulatory enzyme in the biosynthesis of starch in spinach leaf chloroplasts. *J. Biol. Chem.* **241**: 4491–4504.
- Gilchris, D.G., Woodin, T.S., Kosuge, T., and Johnson, M.L. (1972). Regulation of aromatic amino acid biosynthesis in higher plants. 1. Evidence for a regulatory form of chorismate mutase in etiolated mung bean seedlings. *Plant Physiol.* **49**: 52–57.
- Gleave, A.P. (1992). A versatile binary vector system with a T-DNA organizational structure conducive to efficient integration of cloned DNA into the plant genome. *Plant Mol. Biol.* **20**: 1203–1207.
- Goodwin, S.M., Kolosova, N., Kish, C.M., Wood, K.V., Dudareva, N., and Jenks, M.A. (2003). Cuticle characteristics and volatile emissions of petals in *Antirrhinum majus*. *Physiol. Plant.* **117**: 435–443.
- Graham, J.W.A., Williams, T.C.R., Morgan, M., Fernie, A.R., Ratcliffe, R.G., and Sweetlove, L.J. (2007). Glycolytic enzymes associate dynamically with mitochondria in response to respiratory demand and support substrate channeling. *Plant Cell* **19**: 3723–3738.
- Grant, G.A. (2006). The ACT domain: A small molecule binding domain and its role as a common regulatory element. *J. Biol. Chem.* **281**: 33825–33829.
- Griesbach, R.J., and Asen, S. (1990). Characterization of the flavonol glycosides in petunia. *Plant Sci.* **70**: 49–56.
- Griesbach, R.J., and Kamo, K.K. (1996). The effect of induced polyploidy on the flavonols of Petunia 'Mitchell'. *Phytochemistry* **42**: 361–363.
- Görlach, J., Raesecke, H., Rentsch, D., Regenass, M., Roy, P., Zala, M., Keel, C., Boller, T., Amrhein, N., and Schmid, J. (1995). Temporally distinct accumulation of transcripts encoding enzymes of the prechorismate pathway in elicitor-treated, cultured tomato cells. *Proc. Natl. Acad. Sci. USA* **92**: 3166–3170.
- Hanson, K.R., and Havir, E.A. (1981). Phenylalanine ammonia lyase. In *Biochemistry of Plants*, Vol. 7, Secondary Plant Products, E.E. Conn, ed (New York: Academic Press), pp. 577–625.
- Harring, T., Streibig, J.C., and Husted, S. (1998). Accumulation of shikimic acid: A technique for screening glyphosate efficacy. *J. Agric. Food Chem.* **46**: 4406–4412.
- Henry, W.B., Shaner, D.L., and West, M.S. (2007). Shikimate accumulation in sunflower, wheat, and proso millet after glyphosate application. *Weed Sci.* **55**: 1–5.
- Herrmann, K.M. (1995). The shikimate pathway - Early steps in the biosynthesis of aromatic compounds. *Plant Cell* **7**: 907–919.
- Herrmann, K.M., and Weaver, L.M. (1999). The shikimate pathway. *Annu. Rev. Plant Physiol.* **50**: 473–503.
- Horsch, R.B., Fry, J.E., Hoffmann, N.L., Eichholtz, D., Rogers, S.G., and Fraley, R.T. (1985). A simple and general method for transferring genes into plants. *Science* **227**: 1229–1231.
- Huber, S.C., and Huber, J.L. (1996). Role and regulation of sucrose-phosphate synthase in higher plants. *Annu. Rev. Plant Physiol.* **47**: 431–444.
- Hübner, S., Hehmann, M., Schreiner, S., Martens, S., Lukacin, R., and Matern, U. (2003). Functional expression of cinnamate 4-hydroxylase from *Ammi majus* L. *Phytochemistry* **64**: 445–452.
- Hudson, G.S., and Davidson, B.E. (1984). Nucleotide sequence and transcription of the phenylalanine and tyrosine operons of *Escherichia coli* K12. *J. Mol. Biol.* **180**: 1023–1051.
- Huisman, O.C., and Kosuge, T. (1974). Regulation of aromatic amino acid biosynthesis in higher plants. II. 3-Deoxy-arabino-heptulosonic acid 7-phosphate synthetase from cauliflower. *J. Biol. Chem.* **249**: 6842–6848.
- Jensen, R.A. (1986). The shikimate arogenate pathway - Link between carbohydrate metabolism and secondary metabolism. *Physiol. Plant.* **66**: 164–168.
- Jorin, J., and Dixon, R.A. (1990). Stress responses in Alfalfa (*Medicago sativa* L.). 2. Purification, characterization, and induction of phenylalanine ammonia lyase isoforms from elicitor-treated cell suspension cultures. *Plant Physiol.* **92**: 447–455.
- Jung, E., Zamir, L.O., and Jensen, R.A. (1986). Chloroplasts of higher plants synthesize L-phenylalanine via L-arogenate. *Proc. Natl. Acad. Sci. USA* **83**: 7231–7235.
- Kaminaga, Y., et al. (2006). Plant phenylacetaldehyde synthase is a bifunctional homotetrameric enzyme that catalyzes phenylalanine decarboxylation and oxidation. *J. Biol. Chem.* **281**: 23357–23366.
- Katagiri, M., and Sato, R. (1953). Accumulation of phenylalanine by a phenylalanineless mutant of *Escherichia coli*. *Science* **118**: 250–251.
- Keith, B., Dong, X., Ausubel, F., and Fink, G. (1991). Differential induction of 3-deoxy-D-arabino-heptulosonate 7-phosphate synthase genes in *Arabidopsis thaliana* by wounding and pathogenic attack. *Proc. Natl. Acad. Sci. USA* **88**: 8821–8825.
- Kleeb, A.C., Kast, P., and Hilvert, D. (2006). A monofunctional and thermostable prephenate dehydratase from the archaeon *Methanocaldococcus jannaschii*. *Biochemistry* **45**: 14101–14110.
- Koeduka, T., et al. (2006). Eugenol and isoeugenol, characteristic aromatic constituents of spices, are biosynthesized via reduction of a cinneryl alcohol ester. *Proc. Natl. Acad. Sci. USA* **103**: 10128–10133.
- Koeduka, T., Louie, G., Orlova, I., Kish, C., Ibdah, M., Wilkerson, C., Bowman, M., Baiga, T., Noel, J., Dudareva, N., and Pichersky, E. (2008). The multiple phenylpropene synthases in both *Clarkia breweri* and *Petunia hybrida* represent two distinct protein lineages. *Plant J.* **54**: 362–374.
- Kolosova, N., Gorenstein, N., Kish, C.M., and Dudareva, N. (2001). Regulation of circadian methyl benzoate emission in diurnally and nocturnally emitting plants. *Plant Cell* **13**: 2333–2347.
- Koopmann, E., Logemann, E., and Hahlbrock, K. (1999). Regulation and functional expression of cinnamate 4-hydroxylase from parsley. *Plant Physiol.* **119**: 49–55.
- Liepmann, A.H., and Olsen, L.I. (2004). Genomic analysis of amino-transferases in *Arabidopsis thaliana*. *Crit. Rev. Plant Sci.* **23**: 73–89.
- Long, M., Nagegowda, D., Kaminaga, Y., Ho, K., Kish, C., Schnepf, J., Sherman, D., Weiner, H., Rhodes, D., and Dudareva, N. (2009). Involvement of snapdragon benzaldehyde dehydrogenase in benzoic acid biosynthesis. *Plant J.* **59**: 256–265.
- Marshall Colón, A., Sengupta, N., Rhodes, D., Dudareva, N., and Morgan, J. (2010). A kinetic model describes metabolic response to perturbations and distribution of flux control in the benzenoid network of *Petunia hybrida*. *Plant J.*, in press.
- Nagegowda, D.A., Gutensohn, M., Wilkerson, C.G., and Dudareva, N. (2008). Two nearly identical terpene synthases catalyze the formation of nerolidol and linalool in snapdragon flowers. *Plant J.* **55**: 224–239.
- Negre, F., Kish, C.M., Boatright, J., Underwood, B., Shibuya, K., Wagner, C., Clark, D.G., and Dudareva, N. (2003). Regulation of methylbenzoate emission after pollination in snapdragon and petunia flowers. *Plant Cell* **15**: 2992–3006.
- Ogawa, D., Nakajima, N., Sano, T., Tamaoki, M., Aono, M., Kubo, A., Kanna, M., Ioki, M., Kamada, H., and Saji, H. (2005). Salicylic acid accumulation under O<sub>3</sub> exposure is regulated by ethylene in tobacco plants. *Plant Cell Physiol.* **46**: 1062–1072.
- Ogawa, D., Nakajima, N., Seo, S., Mitsuhashi, I., Kamada, H., and Ohashi, Y. (2006). The phenylalanine pathway is the main route of salicylic acid biosynthesis in tobacco mosaic virus-infected tobacco leaves. *Plant Biotechnol.* **23**: 395–398.
- Orlova, I., Marshall-Colon, A., Schnepf, J., Wood, B., Varbanova, M., Fridman, E., Blakeslee, J.J., Peer, W.A., Murphy, A.S., Rhodes, D., Pichersky, E., and Dudareva, N. (2006). Reduction of benzenoid synthesis in petunia flowers reveals multiple pathways to benzoic acid and enhancement in auxin transport. *Plant Cell* **18**: 3458–3475.

- Pan, Q.H., Zhan, J.C., Liu, H.T., Zhang, J.H., Chen, J.Y., Wen, P.F., and Huang, W.D. (2006). Salicylic acid synthesized by benzoic acid 2-hydroxylase participates in the development of thermotolerance in pea plants. *Plant Sci.* **171**: 226–233.
- Raney, A., Law, G.L., Mize, G.J., and Morris, D.R. (2002). Regulated translation termination at the upstream open reading frame in S-adenosylmethionine decarboxylase mRNA. *J. Biol. Chem.* **277**: 5988–5994.
- Razal, R., Lewis, N., and Towers, G. (1994). Pico-tag analysis of arogenic acid and related free amino acids from plant and fungal extracts. *Phytochem. Anal.* **5**: 98–104.
- Razal, R.A., Ellis, S., Singh, S., Lewis, N.G., and Towers, G.H.N. (1996). Nitrogen recycling in phenylpropanoid metabolism. *Phytochemistry* **41**: 31–35.
- Rios-Esteva, R., and Lange, B.M. (2007). Experimental and mathematical approaches to modeling plant metabolic networks. *Phytochemistry* **68**: 2351–2374.
- Rippert, P., and Matringe, M. (2002). Molecular and biochemical characterization of an *Arabidopsis thaliana* arogenate dehydrogenase with two highly similar and active protein domains. *Plant Mol. Biol.* **48**: 361–368.
- Rippert, P., Puyaubert, J., Grisollet, D., Derrier, L., and Matringe, M. (2009). Tyrosine and phenylalanine are synthesized within the plastids in *Arabidopsis*. *Plant Physiol.* **149**: 1251–1260.
- Roessner, U., Luedemann, A., Brust, D., Fiehn, O., Linke, T., Willmitzer, L., and Fernie, A.R. (2001). Metabolic profiling allows comprehensive phenotyping of genetically or environmentally modified plant systems. *Plant Cell* **13**: 11–29.
- Romero, R.M., Roberts, M.F., and Phillipson, J.D. (1995). Chorismate mutase in microorganisms and plants. *Phytochemistry* **40**: 1015–1025.
- Rubin, J.L., and Jensen, R.A. (1979). Enzymology of L-tyrosine biosynthesis in mung bean (*Vigna radiata* [L.] Wilczek). *Plant Physiol.* **64**: 727–734.
- Savage, L.J., and Ohlrogge, J.B. (1999). Phosphorylation of pea chloroplast acetyl-CoA carboxylase. *Plant J.* **18**: 521–527.
- Sawada, H., Shim, I.S., and Usui, K. (2006). Induction of benzoic acid 2-hydroxylase and salicylic acid biosynthesis - Modulation by salt stress in rice seedlings. *Plant Sci.* **171**: 263–270.
- Schmid, J., and Amrhein, N. (1995). Molecular-organization of the shikimate pathway in higher plants. *Phytochemistry* **39**: 737–749.
- Sheen, J. (2002). A transient expression assay using *Arabidopsis* mesophyll protoplasts. Available at <http://genetics.mgh.harvard.edu/sheenweb/>.
- Siehl, D.L. (1999). The biosynthesis of tryptophan, tyrosine, and phenylalanine from chorismate. In *Plant Amino Acids: Biochemistry and Biotechnology*, B. Singh, ed (New York: CRC Press), pp. 171–204.
- Siehl, D.L., and Conn, E.E. (1988). Kinetic and regulatory properties of arogenate dehydratase in seedlings of *Sorghum bicolor* (L.). *Arch. Biochem. Biophys.* **260**: 822–829.
- Siehl, D.L., Singh, B.K., and Conn, E.E. (1986). Tissue distribution and subcellular localization of prephenate aminotransferase in leaves of *Sorghum bicolor*. *Plant Physiol.* **81**: 711–713.
- Simmonds, S. (1950). The metabolism of phenylalanine and tyrosine in mutant strains of *Escherichia coli*. *J. Biol. Chem.* **185**: 755–762.
- Singh, B., and Shaner, D. (1998). Rapid determination of glyphosate injury to plants and identification of glyphosate resistant plants. *Weed Technol.* **12**: 527–530.
- Suzich, J.A., Dean, J.F.D., and Herrmann, K.M. (1985). 3-Deoxy-D-arabino-heptulosonate 7-phosphate synthase from carrot root (*Daucus carota*) is a hysteretic enzyme. *Plant Physiol.* **79**: 765–770.
- Tamura, K., Dudley, J., Nei, M., and Kumar, S. (2007). MEGA4: Molecular Evolutionary Genetics Analysis (MEGA) software version 4.0. *Mol. Biol. Evol.* **24**: 1596–1599.
- Tetlow, I.J., Wait, R., Lu, Z.X., Akkasaeng, R., Bowsher, C.G., Esposito, S., Kosar-Hashemi, B., Morell, M.K., and Emes, M.J. (2004). Protein phosphorylation in amyloplasts regulates starch branching enzyme activity and protein-protein interactions. *Plant Cell* **16**: 694–708.
- Thomas, S.G., Phillips, A.L., and Hedden, P. (1999). Molecular cloning and functional expression of gibberellin 2-oxidases, multifunctional enzymes involved in gibberellin deactivation. *Proc. Natl. Acad. Sci. USA* **96**: 4698–4703.
- Tzin, V., Malitsky, S., Aharoni, A., and Galili, G. (2009). Expression of a bacterial bi-functional chorismate mutase/prephenate dehydratase modulates primary and secondary metabolism associated with aromatic amino acids in *Arabidopsis*. *Plant J.* **60**: 156–167.
- Uhrig, R.G., She, Y.M., Leach, C.A., and Plaxton, W.C. (2008). Regulatory monoubiquitination of phosphoenolpyruvate carboxylase in germinating castor oil seeds. *J. Biol. Chem.* **283**: 29650–29657.
- Underwood, B.A., Tieman, D.M., Shibuya, K., Dexter, R.J., Loucas, H.M., Simkin, A.J., Sims, C.A., Schmelz, E.A., Klee, H.J., and Clark, D.G. (2005). Ethylene-regulated floral volatile synthesis in petunia corollas. *Plant Physiol.* **138**: 255–266.
- Verdonk, J.C., de Vos, C.H.R., Verhoeven, H.A., Haring, M.A., van Tunen, A.J., and Schuurink, R.C. (2003). Regulation of floral scent production in petunia revealed by targeted metabolomics. *Phytochemistry* **62**: 997–1008.
- Verdonk, J.C., Haring, M.A., van Tunen, A.J., and Schuurink, R.C. (2005). ODORANT1 regulates fragrance biosynthesis in petunia flowers. *Plant Cell* **17**: 1612–1624.
- Waller, J.C., Akhtar, T.A., Lara-Núñez, A., Gregory, J.F., McQuinn, R.P., Giovannoni, J.J., and Hanson, A.D. (2010). Developmental and feedforward control of the expression of folate biosynthesis genes in tomato fruit. *Mol. Plant* **3**: 66–77.
- Wang, Z., and Sachs, M.S. (1997). Ribosome stalling is responsible for arginine-specific translational attenuation in *Neurospora crassa*. *Mol. Cell. Biol.* **17**: 4904–4913.
- Warpeha, K.M., Lateef, S.S., Lapik, Y., Anderson, M., Lee, B.S., and Kaufman, L.S. (2006). G-protein-coupled receptor 1, G-protein G alpha-subunit 1, and prephenate dehydratase 1 are required for blue light-induced production of phenylalanine in etiolated *Arabidopsis*. *Plant Physiol.* **140**: 844–855.
- Wildermuth, M.C., Dewdney, J., Wu, G., and Ausubel, F.M. (2001). Isochorismate synthase is required to synthesize salicylic acid for plant defence. *Nature* **414**: 562–565.
- Winkel, B.S.J. (2004). Metabolic channeling in plants. *Annu. Rev. Plant Biol.* **55**: 85–107.
- Yamada, T., Matsuda, F., Kasai, K., Fukuoka, S., Kitamura, K., Tozawa, Y., Miyagawa, H., and Wakasa, K. (2008). Mutation of a rice gene encoding a phenylalanine biosynthetic enzyme results in accumulation of phenylalanine and tryptophan. *Plant Cell* **20**: 1316–1329.
- Zamir, L., Tiberio, R., and Jensen, R. (1983). Differential acid-catalyzed aromatization of prephenate, arogenate, and spiro-arogenate. *Tetrahedron Lett.* **24**: 2815–2818.
- Zamir, L.O., Tiberio, R., Fiske, M., Berry, A., and Jensen, R.A. (1985). Enzymatic and nonenzymatic dehydration reactions of L-arogenate. *Biochemistry* **24**: 1607–1612.
- Zhang, S., Pohnert, G., Kongsaree, P., Wilson, D.B., Clardy, J., and Ganem, B. (1998). Chorismate mutase-prephenate dehydratase from *Escherichia coli* - Study of catalytic and regulatory domains using genetically engineered proteins. *J. Biol. Chem.* **273**: 6248–6253.

**RNAi Suppression of Arogenate Dehydratase1 Reveals That Phenylalanine Is Synthesized Predominantly via the Arogenate Pathway in Petunia Petals**

Hiroshi Maeda, Ajit K Shasany, Jennifer Schnepf, Irina Orlova, Goro Taguchi, Bruce R. Cooper, David Rhodes, Eran Pichersky and Natalia Dudareva

*PLANT CELL* 2010;22;832-849; originally published online Mar 9, 2010;

DOI: 10.1105/tpc.109.073247

This information is current as of June 5, 2010

<b>Supplemental Data</b>	<a href="http://www.plantcell.org/cgi/content/full/tpc.109.073247/DC1">http://www.plantcell.org/cgi/content/full/tpc.109.073247/DC1</a>
<b>References</b>	This article cites 98 articles, 46 of which you can access for free at: <a href="http://www.plantcell.org/cgi/content/full/22/3/832#BIBL">http://www.plantcell.org/cgi/content/full/22/3/832#BIBL</a>
<b>Permissions</b>	<a href="https://www.copyright.com/ccc/openurl.do?sid=pd_hw1532298X&amp;issn=1532298X&amp;WT.mc_id=pd_hw1532298X">https://www.copyright.com/ccc/openurl.do?sid=pd_hw1532298X&amp;issn=1532298X&amp;WT.mc_id=pd_hw1532298X</a>
<b>eTOCs</b>	Sign up for eTOCs for <i>THE PLANT CELL</i> at: <a href="http://www.plantcell.org/subscriptions/etoc.shtml">http://www.plantcell.org/subscriptions/etoc.shtml</a>
<b>CiteTrack Alerts</b>	Sign up for CiteTrack Alerts for <i>Plant Cell</i> at: <a href="http://www.plantcell.org/cgi/alerts/ctmain">http://www.plantcell.org/cgi/alerts/ctmain</a>
<b>Subscription Information</b>	Subscription information for <i>The Plant Cell</i> and <i>Plant Physiology</i> is available at: <a href="http://www.aspb.org/publications/subscriptions.cfm">http://www.aspb.org/publications/subscriptions.cfm</a>